SMAI-JCM
SMAI Journal of Computational Mathematics

An unconditionally stable staggered pressure correction scheme for the compressible Navier-Stokes equations

Dionysis Grapsas, Raphaèle Herbin, Walid Kheriji & Jean-Claude Latché

Volume 2 (2016), p. 51-97.

<http://smai-jcm.cedram.org/item?id=SMAI-JCM_2016__2__51_0>

SMAI Journal of Computational Mathematics
Vol. 2, 51-97 (2016)

An unconditionally stable staggered pressure correction scheme for the compressible Navier-Stokes equations

Dionysis Grapsas [1]
Raphaèle Herbin [2]
Walid Kheriji [3]
Jean-Claude Latché [4]

[1] Aix Marseille Univ, CNRS, Centrale Marseille, I2M, 13453 Marseille, France
E-mail address: dionysis.grapsas@gmail.com
[2] Aix Marseille Univ, CNRS, Centrale Marseille, I2M, 13453 Marseille, France
E-mail address: raphaele.herbin@univ-amu.fr
[3] IRSN, BP 13115, St-Paul-lez-Durance Cedex, France
E-mail address: kheriji.walid@gmail.com
[4] IRSN, BP 13115, St-Paul-lez-Durance Cedex, France
E-mail address: jean-claude.latche@irsn.fr.

Abstract. In this paper we present a pressure correction scheme for the compressible Navier-Stokes equations. The space discretization is staggered, using either the Marker-And-Cell (MAC) scheme for structured grids, or a nonconforming low-order finite element approximation for general quandrangular, hexahedral or simplicial meshes. For the energy balance equation, the scheme uses a discrete form of the conservation of the internal energy, which ensures that this latter variable remains positive; this relation includes a numerical corrective term, to allow the scheme to compute correct shock solutions in the Euler limit. The scheme is shown to have at least one solution, and to preserve the stability properties of the continuous problem, irrespectively of the space and time steps. In addition, it naturally boils down to a usual projection scheme in the limit of vanishing Mach numbers. Numerical tests confirm its potentialities, both in the viscous incompressible and Euler limits.

Math. classification. 65M08, 76N15, 65M12, 76N19.

Keywords. Compressible Navier-Stokes equations, pressure correction schemes, finite volumes, MAC scheme, finite elements.

Contents

1. Introduction

We build in this paper a numerical scheme for the solution of the compressible Navier-Stokes equations:

$$\partial_t \rho + \mathrm{div}(\rho\, \boldsymbol{u}) = 0, \tag{1.1a}$$

$$\partial_t(\rho\, \boldsymbol{u}) + \mathrm{div}(\rho\, \boldsymbol{u} \otimes \boldsymbol{u}) + \boldsymbol{\nabla} p - \mathrm{div}(\boldsymbol{\tau}(\boldsymbol{u})) = 0, \tag{1.1b}$$

$$\partial_t(\rho\, E) + \mathrm{div}(\rho\, E\, \boldsymbol{u}) + \mathrm{div}(p\, \boldsymbol{u}) + \mathrm{div}(\boldsymbol{q}) = \mathrm{div}(\boldsymbol{\tau}(\boldsymbol{u}) \cdot \boldsymbol{u}), \tag{1.1c}$$

$$E = \frac{1}{2}\, |\boldsymbol{u}|^2 + e, \tag{1.1d}$$

$$p = \wp(\rho, e). \tag{1.1e}$$

where t stands for the time, ρ, $\boldsymbol{u}$, p, E and e are the density, velocity, pressure, total energy and internal energy in the flow, $\boldsymbol{\tau}(\boldsymbol{u})$ stands for the shear stress tensor, $\boldsymbol{q}$ stands for the heat diffusion flux, and the function $\wp$ is the equation of state (EOS). The problem is supposed to be posed over $\Omega \times (0, T)$, where Ω is an open bounded connected subset of $\mathbb{R}^d$, $d \leq 3$ and $(0, T)$ is a finite time interval. This system must be supplemented by suitable boundary conditions, initial conditions and closure relations for the diffusion terms.

For the sake of simplicity, we assume in this paper that the velocity is prescribed to zero on the whole boundary $\partial\Omega$, and that the system is adiabatic:

$$\boldsymbol{u} = 0,\ \boldsymbol{q} \cdot \boldsymbol{n} = 0 \text{ on } \partial\Omega. \tag{1.2}$$

However, the modifications of the scheme and of the theoretical arguments to deal with more general boundary conditions are given in remarks, when useful. Suitable initial conditions must be provided for ρ, e and $\boldsymbol{u}$:

$$\rho(\boldsymbol{x}, 0) = \rho_0(\boldsymbol{x}), \quad e(\boldsymbol{x}, 0) = e_0(\boldsymbol{x}), \quad \boldsymbol{u}(\boldsymbol{x}, 0) = \boldsymbol{u}_0(\boldsymbol{x}), \text{ with } \rho_0 > 0,\ e_0 > 0. \tag{1.3}$$

Finally, the closure relations for $\boldsymbol{\tau}(\boldsymbol{u})$ and q are given by:

$$\boldsymbol{\tau}(\boldsymbol{u}) = \mu(\boldsymbol{\nabla}\boldsymbol{u} + \boldsymbol{\nabla}^t\boldsymbol{u}) - \frac{2\mu}{3}\, \mathrm{div}\boldsymbol{u}\, \boldsymbol{I}, \quad \boldsymbol{q} = -\lambda \boldsymbol{\nabla} e, \tag{1.4}$$

where $\boldsymbol{I}$ denotes the identity matrix and $\lambda, \mu \in L^\infty(\Omega)$ are such that there exists $\underline{\lambda} > 0$ and $\underline{\mu} > 0$ such that $\lambda \geq \underline{\lambda}$ a.e. and $\mu \geq \underline{\mu}$ a.e.. Consequently, the shear stress tensor satisfies:

$$\boldsymbol{\tau}(\boldsymbol{u}) : \boldsymbol{\nabla}\boldsymbol{u} \geq 0,\ \forall \boldsymbol{u} \in \mathbb{R}^d, \tag{1.5}$$

Replacing the total energy E by its expression (1.1d) in (1.1c) and developing some terms, we obtain:

$$\partial_t(\rho e) + \mathrm{div}(\rho e \boldsymbol{u}) + p\,\mathrm{div}\boldsymbol{u} + \mathrm{div}(\boldsymbol{q}) + \frac{1}{2}\partial_t(\rho\,|\boldsymbol{u}|^2) + \frac{1}{2}\mathrm{div}(\rho\,|\boldsymbol{u}|^2\,\boldsymbol{u}) + \boldsymbol{u}\cdot\boldsymbol{\nabla}p - \mathrm{div}(\boldsymbol{\tau}(\boldsymbol{u}))\cdot\boldsymbol{u} = \boldsymbol{\tau}(\boldsymbol{u}) : \boldsymbol{\nabla}\boldsymbol{u}. \tag{1.6}$$

Thanks to the mass balance equation (1.1a), we get formally, for any function z:

$$\partial_t(\rho z) + \mathrm{div}(\rho z \boldsymbol{u}) = \rho\,\partial_t z + \rho\boldsymbol{u}\cdot\boldsymbol{\nabla}z.$$

Using this identity twice and then the momentum balance equation (1.1b), we have for $1 \le i \le 3$:

$$\frac{1}{2}\partial_t(\rho u_i^2) + \frac{1}{2}\mathrm{div}(\rho u_i^2\boldsymbol{u}) = \rho u_i\partial_t u_i + \rho u_i\boldsymbol{u}\cdot\boldsymbol{\nabla}u_i = u_i\,\left[\rho\partial_t u_i + \rho\boldsymbol{u}\cdot\boldsymbol{\nabla}u_i\right] = u_i\,\left[\partial_t(\rho u_i) + \mathrm{div}(\rho u_i\boldsymbol{u})\right] = -u_i\,\partial_i p + u_i\,\mathrm{div}(\boldsymbol{\tau}(\boldsymbol{u}))_i,$$

so, summing for $i = 1$ to d:

$$\frac{1}{2}\partial_t(\rho\,|\boldsymbol{u}|^2) + \frac{1}{2}\mathrm{div}(\rho\,|\boldsymbol{u}|^2\,\boldsymbol{u}) = \boldsymbol{u}\cdot\left[\partial_t(\rho\boldsymbol{u}) + \mathrm{div}(\rho\boldsymbol{u}\otimes\boldsymbol{u})\right] = -\boldsymbol{u}\cdot\boldsymbol{\nabla}p + \mathrm{div}(\boldsymbol{\tau}(\boldsymbol{u}))\cdot\boldsymbol{u}.$$

Using this last relation in the total energy equation (1.6) yields the internal energy balance:

$$\partial_t(\rho e) + \mathrm{div}(\rho e\boldsymbol{u}) - \mathrm{div}(\boldsymbol{q}) + p\,\mathrm{div}(\boldsymbol{u}) = \boldsymbol{\tau}(\boldsymbol{u}) : \boldsymbol{\nabla}\boldsymbol{u}. \tag{1.7}$$

Since we assume that the initial condition for ρ is positive, the mass balance (1.1a) implies that the density ρ remains non-negative. Let us now suppose that the equation of state (1.1e) is such that $\wp(\cdot,0) = 0$ and $\wp(0,\cdot) = 0$, which allows to extend $\wp$ by continuity to $\mathbb{R}^2$ (without change of notation):

$$p = \wp(\rho, e), \text{ with } \wp(\rho, e) = 0 \text{ whenever } \rho \le 0 \text{ or } e \le 0. \tag{1.8}$$

Equation (1.7) then implies (thanks to (1.5)) that the internal energy e remains non-negative (at least formally).

Integrating now (1.1c) over Ω yields:

$$\frac{d}{dt}\int_\Omega (\frac{1}{2}\rho\,|\boldsymbol{u}|^2 + \rho e)\,\mathrm{d}\boldsymbol{x} = 0, \tag{1.9}$$

and, since $\rho \ge 0$ and $e \ge 0$, this inequality provides a stability estimate for the system.

In this paper, we propose and study a pressure correction scheme based on staggered-in-space discretizations (low order non-conforming finite elements or MAC scheme), solving the internal energy balance (1.7) instead of the total energy conservation equation (1.1d). As a consequence of these choices, this algorithm naturally boils down to a standard projection method in the vanishing Mach number (*i.e.* incompressible) asymptotic limit. We are able to prove, for this scheme, the same stability properties as in the continuous case: the approximate density and internal energy are non-negative (in fact, for discrete solutions, positive) and a discrete analogue to Relation (1.9) is derived. As a consequence of these properties, we are also able to prove the existence of a solution of the scheme.

This algorithm was already introduced in [20], for the Euler equations only, and its consistency (in the Lax-Wendroff sense) was proven in [20] in one space dimension. We complement this work here in several directions: we extend the scheme to the Navier-Stokes equations, prove the positivity of the internal energy and the existence of a solution to the scheme (while these properties are only claimed in [20]), provide some implementation details and some qualitative properties of the scheme (in particular, clarify its behaviour at contact discontinuities) and present two and three-dimensional numerical experiments, including a test to assess the behaviour in the low Mach number limit.

The fractional step strategy that we consider here involves an elliptic pressure correction step; this strategy has been used for compressible flows to obtain algorithms which are not limited by stringent stability conditions (such as CFL conditions based on the celerity of the fastest waves) since the late sixties, when first attempts were done to build "all flow velocity" schemes [17, 18]; these algorithms may be seen as an extension to the compressible case of the celebrated MAC scheme, introduced some years before [19]. These seminal papers have been the starting point for the development of numerous schemes falling in the class of pressure correction algorithms (possibly iterative, in the spirit of the SIMPLE method), some of them based on staggered finite volume space discretizations [4, 24, 25, 44, 26, 34, 1, 50, 8, 42, 47, 46, 43, 45, 30]; a bibliography extended to the schemes using other space discretizations may be found in [20]. To the best of our knowledge, the present paper provides the first rigorous stability proof for such algorithms in the framework of the Navier-Stokes equations. A key ingredient is the possibility to work with the internal energy balance to ensure the positivity of this quantity, without losing the consistency with the conservative equations (including the total energy balance) in the Euler case. Note also that, for the MAC scheme, a careful design of the viscous dissipation term is necessary to satisfy a discrete analogue of (1.5) (Section 3.2). Finally, the stability of the scheme also relies on the possibility to derive a local discrete kinetic energy balance, for which a rescaling step of the pressure gradient was introduced in [20]. Note also that the scheme proposed in this work implements a staggered finite-volume approach for first order terms (known for its efficiency) while being able to cope with unstructured meshes.

This paper is structured as follows. We first describe the space discretization (Section 2), then the scheme (Section 3). Section 4 is devoted to the proof of stability and existence of discrete solutions. Numerical tests are presented in Section 5. Since the scaling of the pressure gradient allowing to derive a discrete kinetic energy balance may be extended to other discretizations, we present the essential arguments for its design in a time-discrete (and space-continuous) setting in Appendix A. The behaviour of the scheme on contact discontinuities of the Euler equations is adressed in Appendix B. Finally, in Appendix C, we provide some details about the numerical solution of the nonlinear algebraic system associated to the pressure correction step; we also discuss the issue of spurious pressure boundary conditions which are known to be inherent to the pressure correction time-splitting technique.

2. **Meshes and unknowns**

Let $\mathcal{M}$ be a decomposition of the domain Ω, supposed to be regular in the usual sense of the finite element literature (*e.g.* [5]). The cells may be:

- for a general domain Ω, either convex quadrilaterals ($d = 2$) or hexahedra ($d = 3$) or simplices, both types of cells being possibly combined in a same mesh in two space dimensions,

- for a domain whose boundaries are hyperplanes normal to a coordinate axis, rectangles ($d = 2$) or rectangular parallelepipeds ($d = 3$) (the faces of which, of course, are then also necessarily normal to a coordinate axis).

By $\mathcal{E}$ and $\mathcal{E}(K)$ we denote the set of all $(d-1)$-faces σ of the mesh and of the element $K \in \mathcal{M}$ respectively. The set of faces included in the boundary of Ω is denoted by $\mathcal{E}_{\rm ext}$ and the set of internal faces (*i.e.* $\mathcal{E} \setminus \mathcal{E}_{\rm ext}$) is denoted by $\mathcal{E}_{\rm int}$. A face $\sigma \in \mathcal{E}_{\rm int}$ separating the cells K and L is denoted by $\sigma = K|L$. The outward normal vector to a face σ of K is denoted by $\boldsymbol{n}_{K,\sigma}$. For $1 \leq i \leq d$, we denote by $\mathcal{E}^{(i)}$, $\mathcal{E}^{(i)}_{\rm int}$ and $\mathcal{E}^{(i)}_{\rm ext}$ the subset of the faces of $\mathcal{E}$, $\mathcal{E}_{\rm int}$ and $\mathcal{E}_{\rm ext}$ respectively which are perpendicular to the i^{th} unit vector of the canonical basis of $\mathbb{R}^d$. For $K \in \mathcal{M}$ and $\sigma \in \mathcal{E}$, we denote by $|K|$ the measure of K and by $|\sigma|$ the $(d-1)$-measure of the face σ.

The space discretization is staggered, using either the Marker-And Cell (MAC) scheme [19, 18], or nonconforming low-order finite element approximations, namely the Rannacher and Turek (RT) element [39] for quadrilateral or hexahedral meshes, or the lowest degree Crouzeix-Raviart (CR) element [9] for simplicial meshes.

For all these space discretizations, the degrees of freedom for the pressure, the density and the internal energy (*i.e.* the discrete pressure, density and internal energy unknowns) are associated to the cells of the mesh $\mathcal{M}$, and are denoted by:

$$\{p_K,\ \rho_K,\ e_K,\ K \in \mathcal{M}\}.$$

Let us then turn to the degrees of freedom for the velocity.

- **Rannacher-Turek** or **Crouzeix-Raviart** discretizations – The discrete velocity unknowns are located at the center of the faces of the mesh, and we choose the version of the element where they represent the average of the velocity through a face. The Dirichlet boundary conditions are taken into account by setting the velocity unknowns associated to an external face to zero, so the set of discrete velocity unknowns reads:

$$\{u_{\sigma,i},\ \sigma \in \mathcal{E}_{\rm int},\ 1 \leq i \leq d\}.$$

- **MAC** discretization – The degrees of freedom for the i^{th} component of the velocity are located at the centre of the faces $\sigma \in \mathcal{E}^{(i)}$, so the whole set of discrete velocity unknowns reads:

$$\{u_{\sigma,i},\ \sigma \in \mathcal{E}^{(i)}_{\rm int},\ 1 \leq i \leq d\}.$$

Hence there are d unknowns per face of the primal mesh in the case of the CR-RT scheme, namely the d components of the velocity, while there is only one unknown per face of the primal mesh in the case of the MAC scheme, namely the normal component of the velocity.

We now introduce a dual mesh, for the finite volume approximation of the time derivative and convection terms in the momentum balance equation.

- **Rannacher-Turek** or **Crouzeix-Raviart** discretizations – For the RT or CR discretizations, the dual mesh is the same for all the velocity components. When $K \in \mathcal{M}$ is a simplex, a rectangle or a cuboid, for $\sigma \in \mathcal{E}(K)$, we define $D_{K,\sigma}$ as the cone with basis σ and with vertex the mass center of K (see Figure 2.1). We thus obtain a partition of K in m sub-volumes, where m is the number of faces of the cell, each sub-volume having the same measure $|D_{K,\sigma}| = |K|/m$. We extend this definition to general quadrangles and hexahedra, by supposing that we have built a partition still of equal-volume sub-cells, and with the same connectivities. The volume $D_{K,\sigma}$ is referred to as the half-diamond cell associated to K and σ. For $\sigma \in \mathcal{E}_{\rm int}$, $\sigma = K|L$, we now define the diamond cell D_σ associated to σ by $D_\sigma = D_{K,\sigma} \cup D_{L,\sigma}$.

- **MAC** discretization – For the MAC scheme, the dual mesh depends on the component of the velocity. For each component, the MAC dual mesh only differs from the RT or CR dual mesh by the choice of the half-diamond cell, which, for $K \in \mathcal{M}$ and $\sigma \in \mathcal{E}(K)$, is now the rectangle or rectangular parallelepiped of basis σ and of measure $|D_{K,\sigma}| = |K|/2$ (see Figures 3.1 and 3.2).

We denote by $|D_\sigma|$ the measure (area of volume) of the dual cell D_σ, and by $\varepsilon = D_\sigma|D_{\sigma'}$ the face separating two diamond cells D_σ and $D_{\sigma'}$. The set of the (dual) faces of D_σ is denoted by $\bar{\mathcal{E}}(D_\sigma)$.

Finally, in order to be able to write a unique expression of the discrete equations for both MAC and CR/RT schemes, we introduce the set of faces $\mathcal{E}_{\rm s}^{(i)}$ associated to the degrees of freedom of the i^{th}

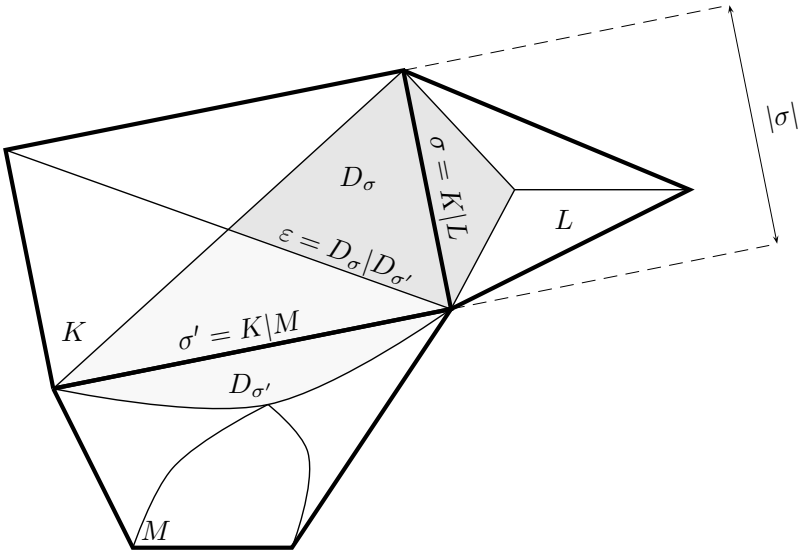

Figure 2.1. Primal and dual meshes for the Rannacher-Turek and Crouzeix-Raviart elements.

component of the velocity ($\mathcal{S}$ stands for "scheme"):

$$\mathcal{E}_{\mathcal{S}}^{(i)} = \left| \begin{array}{l} \mathcal{E}_{\rm int}^{(i)} \text{ for the MAC scheme,} \\ \mathcal{E}_{\rm int} \text{ for the CR or RT schemes.} \end{array} \right.$$

In addition, for the definition of the discrete diffusion terms in the momentum balance equation (1.1b) and in the internal energy equation (1.7), we need to distinguish two classes of meshes: the so-called super-admissible meshes, and the others, referred to as general meshes. In the present particular framework, super-admissible meshes are obtained under the following condition:

$$\left| \begin{array}{l} \text{Each cell } K \text{ of the mesh is either:} \\ \quad \text{- a rectangle } (d=2) \text{ or a rectangular parallelepiped } (d=3); \text{ in this} \\ \quad\ \ \text{case, we denote by } \boldsymbol{x}_K \text{ the mass center of } K; \\ \quad \text{- a simplex, the circumcenter } \boldsymbol{x}_K \text{ of which is located inside } K. \end{array} \right. \tag{2.1}$$

This condition implies that, for each neighboring control volumes K and L, the segment $[x_K, x_L]$ is orthogonal to the face $K|L$ separating K from L, even when, in two space dimensions, one cell is a rectangle and the other one a triangle (we recall that, in three space dimensions, the two types of cells cannot be mixed). For each internal face $\sigma = K|L$, we denote by d_σ the distance $d(x_K, x_L)$.

Remark 2.1 (Impermeability and Neumann boundary conditions)**.** If the velocity is not prescribed to zero at the boundary, the space discretization is adapted as follows:

- if $\boldsymbol{u}\cdot\boldsymbol{n} = 0$ is the only condition imposed on the boundary, the degrees of freedom do not change for the MAC scheme, but the velocity unknowns corresponding to the tangential component(s) of the velocity must be added for the RT and CR discretizations. We thus first need a definition of the dual cell at a boundary face $\sigma \in \mathcal{E}_{\rm ext}$; denoting by K the adjacent cell, we take for D_σ the same volume as $D_{K,\sigma}$. Next, we must extend $\mathcal{E}_{\mathcal{S}}^{(i)}$. This can be done in a straightforward way if the boundary is always normal to a vector of the canonical basis of $\mathbb{R}^d$; then we get

$\mathcal{E}_{\rm S}^{(i)} = \mathcal{E} \setminus \mathcal{E}_{\rm ext}^{(i)}$. This is the situation that we will consider here. The extension to the general case is just technical: a change of unknown must be done to make the velocity in the direction normal to each external face appear as a degree of freedom.

- when the velocity is free at a boundary face σ, this face must be treated in the definition of $\mathcal{E}_{\rm S}^{(i)}$ as an internal face, and the associated dual cell is defined as previously.

3. The pressure correction scheme

3.1. The algorithm

Let us consider a partition $0 = t_0 < t_1 < \ldots < t_N = T$ of the time interval $(0, T)$, which we suppose uniform. Let $\delta t = t_{n+1} - t_n$ for $n = 0, 1, \ldots, N-1$ be the constant time step. The pressure correction scheme considered here consists in the two following steps:

Pressure gradient scaling step:

$$\forall \sigma \in \mathcal{E}_{\rm int}, \quad \overline{\boldsymbol{\nabla}}_\sigma(p^{n+1}) = \Big(\frac{\rho^n_{D_\sigma}}{\rho^{n-1}_{D_\sigma}}\Big)^{1/2} \boldsymbol{\nabla}_\sigma(p^n). \tag{3.1a}$$

Prediction step – Solve for $\tilde{\boldsymbol{u}}^{n+1}$:

For $1 \le i \le d$, $\forall \sigma \in \mathcal{E}_{\rm S}^{(i)}$,

$$\frac{1}{\delta t}\,(\rho^n_{D_\sigma}\tilde{u}^{n+1}_{\sigma,i} - \rho^{n-1}_{D_\sigma}u^n_{\sigma,i}) + {\rm div}_\sigma(\rho^n\tilde{u}^{n+1}_i\boldsymbol{u}^n) - {\rm div}_{\sigma,i}\,\boldsymbol{\tau}(\tilde{\boldsymbol{u}}^{n+1}) + \overline{\boldsymbol{\nabla}}_{\sigma,i}(p^{n+1}) = 0. \tag{3.1b}$$

Correction step – Solve for p^{n+1}, e^{n+1}, ρ^{n+1} and $\boldsymbol{u}^{n+1}$:

For $1 \le i \le d$, $\forall \sigma \in \mathcal{E}_{\rm S}^{(i)}$,

$$\frac{1}{\delta t}\,\rho^n_{D_\sigma}\,(u^{n+1}_{\sigma,i} - \tilde{u}^{n+1}_{\sigma,i}) + \boldsymbol{\nabla}_{\sigma,i}(p^{n+1}) - \overline{\boldsymbol{\nabla}}_{\sigma,i}(p^{n+1}) = 0, \tag{3.1c}$$

$$\forall K \in \mathcal{M}, \quad \frac{1}{\delta t}(\rho^{n+1}_K - \rho^n_K) + {\rm div}_K(\rho^{n+1}\boldsymbol{u}^{n+1}) = 0, \tag{3.1d}$$

$\forall K \in \mathcal{M}$,

$$\begin{aligned}\frac{1}{\delta t}(\rho^{n+1}_K e^{n+1}_K - \rho^n_K e^n_K) + {\rm div}_K(\rho^{n+1}e^{n+1}\boldsymbol{u}^{n+1}) + p^{n+1}_K\,{\rm div}_K(\boldsymbol{u}^{n+1}) \\ -\lambda\,(\Delta e^{n+1})_K = \big(\boldsymbol{\tau}(\tilde{\boldsymbol{u}}^{n+1}) : \boldsymbol{\nabla}\tilde{\boldsymbol{u}}^{n+1}\big)_K + S^{n+1}_K,\end{aligned} \tag{3.1e}$$

$$\forall K \in \mathcal{M}, \quad \rho^{n+1}_K = \varrho(e^{n+1}_K, p^{n+1}_K). \tag{3.1f}$$

The first step is a pressure gradient scaling step which is introduced in order to recover a discrete kinetic energy inequality (see Appendix A). The second step is a classical semi-implicit solution of the momentum balance equation to obtain a tentative velocity field. The third step is a nonlinear pressure correction step, which couples the mass balance equation with the internal energy balance equation. However expensive, this coupling seems to be the price to pay to obtain an unconditional stability property (see Section 4.1, and [36, 37] for a discussion on this issue). In addition, in the Euler case, it also allows the scheme to keep the velocity and pressure constant across (1D) contact discontinuities

(see Appendix B). The last equation of this step is the equation of state, which is recast here as $\rho = \varrho(e,p)$ (instead of $p = \wp(\rho,e)$) because, at the algebraic level, the density is first eliminated from the system, this latter is solved for e^{n+1} and p^{n+1}, and ρ^{n+1} is finally given by (3.1f) (see Appendix C for the solution process).

We now give the expression of each term of this algorithm, except for the diffusion and dissipation terms, which are defined in sections 3.2 and 3.3 below. The space discretization follows a specific order, which is explained in Flow chart 3.1 below.

(i) (For the mass balance) Define the mass flux at each primal face:

$$\mathrm{div}_K(\rho\boldsymbol{u}) = \frac{1}{|K|}\sum_{\sigma\in\mathcal{E}(K)} F_{K,\sigma}, \quad F_{K,\sigma} = |\sigma|\ \rho_\sigma\ u_{K,\sigma},$$

$u_{K,\sigma}$ =normal velocity, ρ_σ =upwind density (*ensures the positivity of the density*).

(ii) From this primal mass flux,

(a) (For the momentum balance) Define the density at the faces ρ_{D_σ} and the mass fluxes through the dual faces $F_{\sigma,\varepsilon}$ in such a way that a mass balance holds on dual cells, and define the flux of the i^{th} velocity component through a dual face by $F_{\sigma,\varepsilon}u_{\varepsilon,i}$, with $u_{\varepsilon,i}$ centered (*yields a discrete kinetic energy balance*);

(b) (For the internal energy balance) Define the energy flux through each primal face by $F_{K,\sigma}\,e_\sigma$, with e_σ =upwind energy (*yields a maximum-principle-preserving convection operator*);

(c) (For the internal energy balance) Define the velocity divergence (just set ρ equal to 1 in the expression of $\mathrm{div}_K(\rho\boldsymbol{u})$), and the pressure gradient by transposition (*yields a total energy estimate*).

Flow chart 3.1. Process for the construction of the space discretization of the hyperbolic part of the system of partial differential equations (*i.e.* Euler equations, written in non-conservative form using the internal energy balance). This process must be combined with a time stepping strategy which, in practice, may be of pressure correction type (present paper, to ensure unconditional stability) or explicit (see [22]).

We begin with the discrete mass balance equation (3.1d). The convection term in this relation reads:

$$\mathrm{div}(\rho\boldsymbol{u})_K = \frac{1}{|K|}\sum_{\sigma\in\mathcal{E}(K)} F_{K,\sigma},$$

where $F_{K,\sigma}$ stands for the mass flux across σ outward K. By the impermeability boundary conditions, it vanishes on external faces and is given on internal faces by:

$$\forall\sigma\in\mathcal{E}_{\rm int},\ \sigma = K|L, \qquad F_{K,\sigma} = |\sigma|\ \rho_\sigma\ u_{K,\sigma}, \tag{3.2}$$

where $u_{K,\sigma}$ is an approximation of the normal velocity to the face σ outward K. This latter quantity is defined by:

$$u_{K,\sigma} = \begin{vmatrix} u_{\sigma,i}\ \boldsymbol{n}_{K,\sigma}\cdot\boldsymbol{e}^{(i)} \text{ for } \sigma\in\mathcal{E}^{(i)} \text{ in the MAC case,} \\ \boldsymbol{u}_\sigma\cdot\boldsymbol{n}_{K,\sigma} \text{ in the CR and RT cases,} \end{vmatrix} \tag{3.3}$$

where $\boldsymbol{e}^{(i)}$ denotes the i-th vector of the orthonormal basis of $\mathbb{R}^d$. The density at the face $\sigma = K|L$ is approximated by the upwind technique, *i.e.* $\rho_\sigma = \rho_K$ if $u_{K,\sigma}\geq 0$ and $\rho_\sigma = \rho_L$ otherwise.

We now turn to the discrete momentum balance (3.1b). For both the MAC and the RT-CR discretizations, the time derivative and convection terms are approximated in (3.1b) by a finite volume technique over the dual cells, so that the convection term reads:

$$\mathrm{div}_\sigma(\rho\tilde{u}_i\boldsymbol{u}) = \mathrm{div}_\sigma\big(\tilde{u}_i(\rho\boldsymbol{u})\big) = \frac{1}{|D_\sigma|}\sum_{\varepsilon\in\bar{\mathcal{E}}(D_\sigma)} F_{\sigma,\varepsilon}\tilde{u}_{\varepsilon,i},$$

where $F_{\sigma,\varepsilon}$ stands for a mass flux through the dual face ε outward D_σ, and $\tilde{u}_{\varepsilon,i}$ is a centered approximation of the i^{th} component of the velocity $\tilde{\boldsymbol{u}}$ on ε. The density at the dual cell ρ_{D_σ} is obtained by a weighted average of the density in the neighbouring cells:

$$\begin{aligned} &\text{for } \sigma\in\mathcal{E}_{\rm int},\ \sigma = K|L, && |D_\sigma|\,\rho_{D_\sigma} = |D_{K,\sigma}|\,\rho_K + |D_{L,\sigma}|\,\rho_L,\\ &\text{for an external face of a cell } K, && \rho_{D_\sigma} = \rho_K. \end{aligned} \tag{3.4}$$

The mass fluxes $(F_{\sigma,\varepsilon})_{\varepsilon\in\mathcal{E}(D_\sigma)}$ are evaluated as linear combinations, with constant coefficients, of the primal mass fluxes at the neighboring faces, in such a way that the following discrete mass balance over the dual cells is implied by the discrete mass balance (3.1d):

$$\forall\sigma\in\mathcal{E},\ \text{for } 0\le n<N, \qquad \frac{|D_\sigma|}{\delta t}\,(\rho_{D_\sigma}^{n+1}-\rho_{D_\sigma}^{n}) + \sum_{\varepsilon\in\mathcal{E}(D_\sigma)} F_{\sigma,\varepsilon}^{n+1} = 0. \tag{3.5}$$

This relation is critical to derive a discrete kinetic energy balance (see Section 4.1 below). The computation of the dual mass fluxes $F_{\sigma,\varepsilon}$ is such that the flux through a dual face lying on the boundary, which is then also a primal face, is the same as the primal flux, that is zero. This computation yields the expression (3.4) for the densities, and some linear combination of the primal fluxes for the dual fluxes [13, 20, 21]. Since the mass balance is not yet solved at the velocity prediction stage, the densities and dual fluxes have to be built from the mass balance at the previous time step: hence the backward time shift for the densities in the time-derivative term.

In the rescaling step for the pressure gradient (3.1a) and in the correction equation (3.1c), the term $\boldsymbol{\nabla}_{\sigma,i}(p)$ stands for the i^{th} component of the discrete pressure gradient at the face σ, which is built as the transposed operator to the natural divergence (see Equations (3.8) and (3.9) below):

$$\text{for } \sigma = K|L\in\mathcal{E}_{\rm int}, \qquad \boldsymbol{\nabla}_{\sigma,i}(p) = \frac{|\sigma|}{|D_\sigma|}\,(p_L-p_K)\,\boldsymbol{n}_{K,\sigma}\cdot\boldsymbol{e}^{(i)}. \tag{3.6}$$

This pressure gradient is only defined at internal faces since, thanks to the impermeability boundary conditions, no momentum balance equation is written at the external faces. The quantity $\overline{\boldsymbol{\nabla}}_{\sigma,i}(p)$ in (3.1a) is obtained by a simple rescaling of the pressure gradient, which is needed to obtain a discrete kinetic energy balance (see Section 4.1 and Appendix A). Note that $\overline{\boldsymbol{\nabla}}(p)$ is not a discrete gradient, in the sense that there does not exist in the general case a discrete pressure $\overline{p}$ such that $\overline{\boldsymbol{\nabla}}(p) = \boldsymbol{\nabla}(\overline{p})$.

Equation (3.1e) is a finite-volume approximation of the internal energy balance over the primal cell K. To ensure the positivity of the convection operator, the convection flux is defined as the product of the mass flux with an upwind approximation of the internal energy [31]:

$$\mathrm{div}_K(\rho e\boldsymbol{u}) = \mathrm{div}_K\big(e\,(\rho\boldsymbol{u})\big) = \frac{1}{|K|}\sum_{\sigma\in\mathcal{E}(K)} F_{K,\sigma}e_\sigma, \tag{3.7}$$

with, for $\sigma = K|L\in\mathcal{E}_{\rm int}$, $e_\sigma = e_K$ if $F_{K,\sigma}\ge 0$ and $e_\sigma = e_L$ otherwise. The divergence of the velocity, $\mathrm{div}_K(\boldsymbol{u})$, is discretized as follows:

$$\text{for } K\in\mathcal{M}, \qquad \mathrm{div}_K(\boldsymbol{u}) = \frac{1}{|K|}\sum_{\sigma\in\mathcal{E}(K)} |\sigma|\,u_{K,\sigma}, \tag{3.8}$$

and, as announced, this definition implies that the discrete gradient and divergence operators are dual with respect to the L^2 inner product:

$$\sum_{K\in\mathcal{M}} |K|\ p_K\ \mathrm{div}_K(\boldsymbol{u}) + \sum_{i=1}^{d} \sum_{\sigma\in\mathcal{E}_{\mathrm{S}}^{(i)}} |D_\sigma|\ u_{\sigma,i}\ \boldsymbol{\nabla}_{\sigma,i}(p) = 0. \tag{3.9}$$

The term S_K at the right-hand side of (3.1e) is necessary to obtain a consistent scheme in the Euler case [20]; its purpose is to compensate some numerical dissipation terms appearing in the discrete kinetic energy balance equation, which may not tend to 0 as the mesh and time step tend to 0. Its expression is derived in Section 4.1.

Remark 3.1 (Outflow or Neuman boundary conditions)**.** When the normal velocity is not prescribed to zero at the boundary face $\sigma \in \mathcal{E}(K)$, we suppose that the flow leaves the domain (*i.e.* $u_{K,\sigma} \geq 0$), so the definition (3.2) of $F_{K,\sigma}$ remains unchanged (and $\rho_\sigma = \rho_K$). The face σ is also an external dual face of the diamond cell D_σ, and the above mentioned construction procedure of the dual mass fluxes yields $F_{\sigma,\varepsilon} = F_{K,\sigma}$; at this face, we set $\tilde{u}_{\varepsilon,i} = \tilde{u}_{\sigma,i}$. The expression (3.8) of the discrete divergence of the velocity still holds, but now takes into account a (possibly) non-zero normal velocity $u_{K,\sigma}$ at the external face σ. Therefore, the gradient-divergence duality property becomes:

$$\sum_{K\in\mathcal{M}} |K|\ p_K\ \mathrm{div}_K(\boldsymbol{u}) + \sum_{i=1}^{d} \sum_{\sigma\in\mathcal{E}_{\mathrm{S}}^{(i)}} |D_\sigma|\ u_{\sigma,i}\ \boldsymbol{\nabla}_{\sigma,i}(p) = \sum_{\sigma\in\mathcal{E}_{\mathrm{ext}}} -|\sigma|\ p_{\mathrm{ext}}$$

where p_{ext} stands for the external pressure involved in the Neumann boundary condition, and we have supposed that the Neumann boundary condition is applied on the whole boundary (otherwise, the sum at the right-hand side should be restricted to the faces included in the part of $\partial\Omega$ where Neumann boundary conditions are prescribed). We thus obtain the following definition of the gradient on the external face σ adjacent to the cell K:

$$\boldsymbol{\nabla}_{\sigma,i}(p^{n+1}) = \frac{|\sigma|}{|D_\sigma|}\ (p_{\mathrm{ext}} - p_K^{n+1})\ \boldsymbol{n}_{K,\sigma}\cdot\boldsymbol{e}^{(i)}.$$

Finally, the definition of the internal energy flux (3.7) remains unchanged (and $e_\sigma = e_K$).

In order to obtain a stability estimate, the dual mass balance (3.5) has to be satisfied when performing the first velocity prediction step, and this complicates the initialization of the scheme. The initial approximations for ρ, e and $\boldsymbol{u}$ are given by the average of the initial conditions ρ_0, e_0 and $\boldsymbol{u}_0$ on the primal and dual cells respectively:

$$\begin{aligned} &\forall K\in\mathcal{M},\quad \rho_K^{(-1)} = \frac{1}{|K|}\int_K \rho_0(\boldsymbol{x})\,\mathrm{d}\boldsymbol{x}, \qquad e_K^0 = \frac{1}{|K|}\int_K e_0(\boldsymbol{x})\,\mathrm{d}\boldsymbol{x}, \\ &\text{for } 1\leq i\leq d,\ \forall\sigma\in\mathcal{E}_{\mathrm{S}}^{(i)},\quad u_{\sigma,i}^0 = \frac{1}{|D_\sigma|}\int_{D_\sigma} (\boldsymbol{u}_0(\boldsymbol{x}))_i\,\mathrm{d}\boldsymbol{x}. \end{aligned} \tag{3.10}$$

Then the discrete mass balance (3.1d), written for $n=-1$, is solved for ρ^0, and the initial pressure is given by the equation of state (1.1e).

3.2. **The viscous diffusion and dissipation term**

The aim of this section is to define the viscous diffusion term $\mathrm{div}_{\sigma,i}\,\boldsymbol{\tau}(\tilde{\boldsymbol{u}})$ of the momentum balance equation (3.1b) and the viscous dissipation term $(\boldsymbol{\tau}(\tilde{\boldsymbol{u}}) : \boldsymbol{\nabla}\tilde{\boldsymbol{u}})_K$ of the internal energy balance equation. Besides usual numerical consistency considerations, we would like these quantities to satisfy the two following constraints:

(*i*) non-negativity of the dissipation:

$$\forall K \in \mathcal{M}, \quad (\boldsymbol{\tau}(\tilde{\boldsymbol{u}}) : \boldsymbol{\nabla}\tilde{\boldsymbol{u}})_K \geq 0; \tag{3.11}$$

(*ii*) consistency of the diffusion and the dissipation, in the following sense:

$$-\sum_{i=1}^{d} \sum_{\sigma \in \mathcal{E}_{\mathrm{S}}^{(i)}} |D_\sigma| \ \mathrm{div}_{\sigma,i}\, \boldsymbol{\tau}(\tilde{\boldsymbol{u}})\ u_{\sigma,i} = \sum_{K \in \mathcal{M}} |K| \ (\boldsymbol{\tau}(\tilde{\boldsymbol{u}}) : \boldsymbol{\nabla}\tilde{\boldsymbol{u}})_K\,, \tag{3.12}$$

i.e. the discrete analogue of the identity $\displaystyle\int_\Omega \mathrm{div}\boldsymbol{\tau}(\boldsymbol{u}) \cdot \boldsymbol{u} = -\int_\Omega \boldsymbol{\tau}(\boldsymbol{u}) : \boldsymbol{\nabla}\boldsymbol{u}$.

Since the discretization of the diffusion term is different for the RT or CR discretization, on one side, and for the MAC scheme, on the other side, we deal with these two cases separately.

3.2.1. *Unstructured meshes, CR-RT discretization.*

For the RT or CR discretization, we use the usual finite element discretization of the viscous term:

$$-\mathrm{div}_{\sigma,i}\, \boldsymbol{\tau}(\tilde{\boldsymbol{u}}) = -\frac{1}{|D_\sigma|} \sum_{K \in \mathcal{M}} \int_K \boldsymbol{\tau}(\tilde{\boldsymbol{u}}) : \boldsymbol{\nabla}\boldsymbol{\varphi}_\sigma^{(i)}\, \mathrm{d}\boldsymbol{x}, \tag{3.13}$$

where $\boldsymbol{\varphi}_\sigma^{(i)}$ stands for the vector-valued finite element shape function associated to the i^{th} component of the velocity and to the face σ; by definition of the RT or CR finite elements, this shape function reads $\varphi_\sigma \boldsymbol{e}^{(i)}$, where φ_σ is the real-valued function of the approximation space whose mean value is 1 over σ and 0 over the other faces of the mesh.

The dissipation term is given by:

$$(\boldsymbol{\tau}(\tilde{\boldsymbol{u}}) : \boldsymbol{\nabla}\tilde{\boldsymbol{u}})_K = \frac{1}{|K|} \int_K \boldsymbol{\tau}(\tilde{\boldsymbol{u}}) : \boldsymbol{\nabla}\tilde{\boldsymbol{u}}\, \mathrm{d}\boldsymbol{x}. \tag{3.14}$$

The non-negativity of this term is a classical result, which is a consequence of the following elementary computation. By symmetry,

$$\boldsymbol{\tau}(\tilde{\boldsymbol{u}}) : \boldsymbol{\nabla}\tilde{\boldsymbol{u}} = \mu\,(\boldsymbol{\nabla}\tilde{\boldsymbol{u}} + \boldsymbol{\nabla}^t\tilde{\boldsymbol{u}}) : \boldsymbol{\nabla}\tilde{\boldsymbol{u}} - \frac{2\mu}{3}\,\mathrm{div}(\tilde{\boldsymbol{u}})\, \boldsymbol{I} : \boldsymbol{\nabla}\tilde{\boldsymbol{u}} = \mu\,((\boldsymbol{\nabla}\tilde{\boldsymbol{u}} + \boldsymbol{\nabla}^t\tilde{\boldsymbol{u}}) : (\boldsymbol{\nabla}\tilde{\boldsymbol{u}} + \boldsymbol{\nabla}^t\tilde{\boldsymbol{u}}) - \frac{2}{3}\,(\mathrm{div}\tilde{\boldsymbol{u}})^2).$$

This expression is thus the sum of the squares of the off-diagonal entries of $\boldsymbol{\nabla}\tilde{\boldsymbol{u}} + \boldsymbol{\nabla}^t\tilde{\boldsymbol{u}}$ and of the following quantity

$$\frac{2\mu}{3}\Big(3\sum_{i=1}^{3}(\partial_i u_i)^2 - \big(\sum_{i=1}^{3}\partial_i u_i\big)^2\Big),$$

which is non-negative.

Finally, by a simple reordering of the sums,

$$\begin{aligned}
&-\sum_{i=1}^{d} \sum_{\sigma \in \mathcal{E}_{\mathrm{S}}^{(i)}} |D_\sigma| \ \mathrm{div}_{\sigma,i}\, \boldsymbol{\tau}(\tilde{\boldsymbol{u}})\ u_{\sigma,i} \\
&\qquad = \sum_{i=1}^{d} \sum_{\sigma \in \mathcal{E}_{\mathrm{S}}^{(i)}} u_{\sigma,i} \sum_{K \in \mathcal{M}} \int_K \boldsymbol{\tau}(\tilde{\boldsymbol{u}}) : \boldsymbol{\nabla}\boldsymbol{\varphi}_\sigma^{(i)}\, \mathrm{d}\boldsymbol{x} = \sum_{K \in \mathcal{M}} \int_K \boldsymbol{\tau}(\tilde{\boldsymbol{u}}) : \boldsymbol{\nabla}\Big(\sum_{i=1}^{d} \sum_{\sigma \in \mathcal{E}_{\mathrm{S}}^{(i)}} u_{\sigma,i}\boldsymbol{\varphi}_\sigma^{(i)}\Big)\, \mathrm{d}\boldsymbol{x} \\
&\qquad\qquad = \sum_{K \in \mathcal{M}} \int_K \boldsymbol{\tau}(\tilde{\boldsymbol{u}}) : \boldsymbol{\nabla}\tilde{\boldsymbol{u}}\, \mathrm{d}\boldsymbol{x} = \sum_{K \in \mathcal{M}} |K| \ (\boldsymbol{\tau}(\tilde{\boldsymbol{u}}) : \boldsymbol{\nabla}\tilde{\boldsymbol{u}})_K\,,
\end{aligned}$$

that is (3.12).

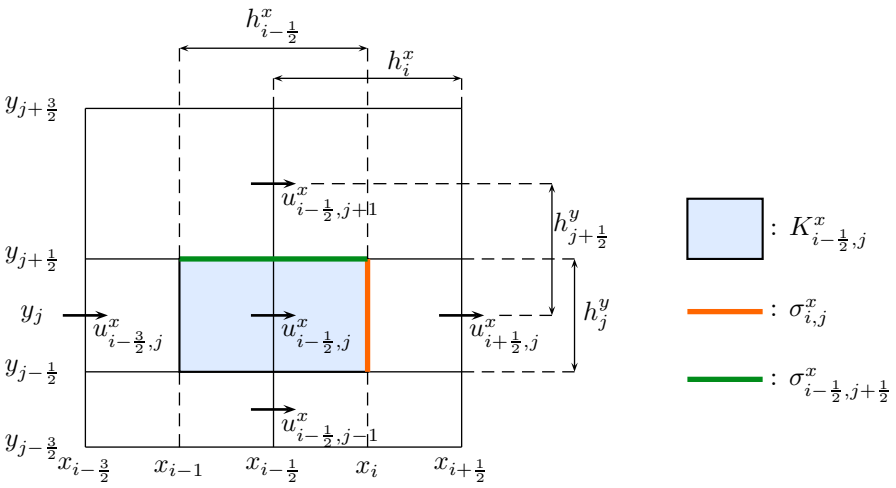

FIGURE 3.1. Unknown and dual cell for the x-component of the velocity, notations for staggered discretizations.

3.2.2. *MAC scheme*

For the MAC scheme, the strategy used to build the viscous diffusion and dissipation terms is to mimic the computation performed in the previous section. Hence, we first need to define the (discrete) partial derivatives of the discrete velocities *a.e* in Ω, and then a finite volume analogue of the shape functions. With these ingredients, expressions (3.13) and (3.14) still make sense, and their consequences (namely Relations (3.11) and (3.12)) hold.

The arguments presented in this section were already used in [13], but with a rather different approach and notations; they are detailed here in the present framework.

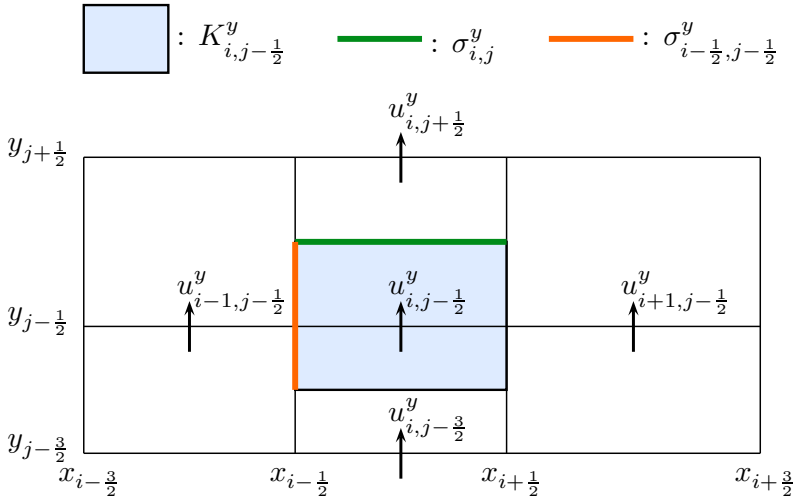

FIGURE 3.2. Unknowns and dual cell for the y-component of the velocity, notations for staggered discretizations (continued).

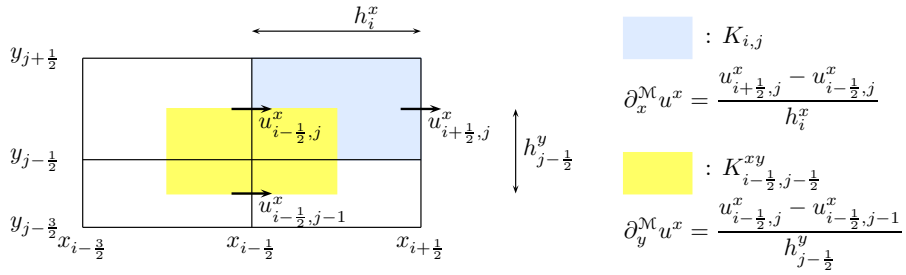

FIGURE 3.3. Discrete partial derivatives of the x-component of the velocity

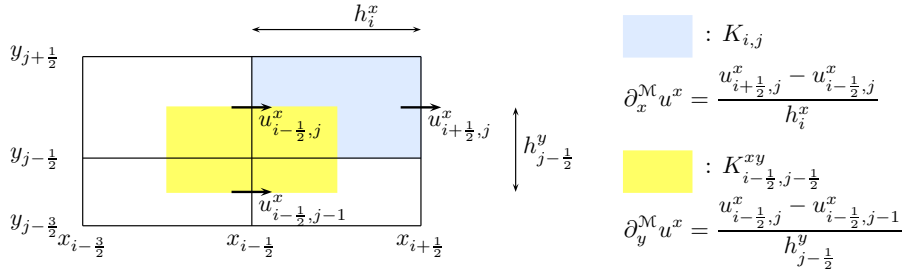

FIGURE 3.4. Discrete partial derivatives of the y-component of the velocity

The two-dimensional case - Since we have to deal with differential quotient formula on structured grids, we use the standard notations in this context given on Figures 3.1 and 3.2. For the sake of clarity, we first concentrate on the inner cells; the cells neighbouring the boundary and the boundary conditions are dealt with later.

The discrete partial derivatives of the velocity are defined as follows (see Figures 3.3 and 3.4):

– Let the primal cells be denoted by $K_{i,j} = (x_{i-1/2}, x_{i+1/2}) \times (y_{j-1/2}, y_{j+1/2})$. The derivatives involved in the divergence, $\partial_x^{\mathcal{M}} u^x$ and $\partial_y^{\mathcal{M}} u^y$, are defined over the primal cell by, $\forall \boldsymbol{x} \in K_{i,j}$:

$$\partial_x^{\mathcal{M}} u^x(\boldsymbol{x}) = \frac{u^x_{i+\frac{1}{2},j} - u^x_{i-\frac{1}{2},j}}{h_i^x}, \quad \partial_y^{\mathcal{M}} u^y(\boldsymbol{x}) = \frac{u^y_{i,j+\frac{1}{2}} - u^y_{i,j-\frac{1}{2}}}{h_j^y}. \tag{3.15}$$

– For the other derivatives, we introduce a fourth mesh which is vertex-centred, and we denote by K^{xy} the generic cell of this new mesh, with $K^{xy}_{i-\frac{1}{2},j-\frac{1}{2}} = (x_{i-1}, x_i) \times (y_{j-1}, y_j)$. Then, $\forall \boldsymbol{x} \in K^{xy}_{i-\frac{1}{2},j-\frac{1}{2}}$:

$$\partial_y^{\mathcal{M}} u^x(\boldsymbol{x}) = \frac{u^x_{i-\frac{1}{2},j} - u^x_{i-\frac{1}{2},j-1}}{h^y_{j-\frac{1}{2}}}, \quad \partial_x^{\mathcal{M}} u^y(\boldsymbol{x}) = \frac{u^y_{i,j-\frac{1}{2}} - u^y_{i-1,j-\frac{1}{2}}}{h^x_{i-\frac{1}{2}}}. \tag{3.16}$$

We are now in position to define the discrete stress tensor of $\tilde{\boldsymbol{u}}$ by:

$$(\mu \boldsymbol{\nabla})^{\mathcal{M}} \tilde{\boldsymbol{u}} = \begin{bmatrix} \mu_{xx}\, \partial_x^{\mathcal{M}} \tilde{u}^x & \mu_{xy}\, \partial_y^{\mathcal{M}} \tilde{u}^x \\ \mu_{yx}\, \partial_x^{\mathcal{M}} \tilde{u}^y & \mu_{yy}\, \partial_y^{\mathcal{M}} \tilde{u}^y \end{bmatrix}, \quad (\mu \operatorname{div})^{\mathcal{M}}(\tilde{\boldsymbol{u}}) = \mu_{xx}\, \partial_x^{\mathcal{M}} \tilde{u}^x + \mu_{yy}\, \partial_y^{\mathcal{M}} \tilde{u}^y,$$

$$\boldsymbol{\tau}^{\mathcal{M}}(\tilde{\boldsymbol{u}}) = (\mu \boldsymbol{\nabla})^{\mathcal{M}} \tilde{\boldsymbol{u}} + \left((\mu \boldsymbol{\nabla}^{\mathcal{M}}) \tilde{\boldsymbol{u}}\right)^t - \frac{2}{3} (\mu \operatorname{div})^{\mathcal{M}} \tilde{\boldsymbol{u}}\, \boldsymbol{I},$$

where μ_{xx}, μ_{xy}, μ_{yx} and μ_{yy} are approximations of the viscosity field on the various meshes; here, we choose to use the same piecewise constant fields for μ_{xx} and μ_{yy} (respectively μ_{xy} and μ_{yx}), with the same mesh as their associated partial derivatives, namely the primal cells (respectively the vertex-centred cells). The value of μ_{xx} and μ_{yy} over $K_{i,j}$ (respectively μ_{xy} and μ_{yx} over $K^{xy}_{i-\frac{1}{2},j-\frac{1}{2}}$) is denoted by $\mu_{i,j}$ (respectively $\mu_{i-\frac{1}{2},j-\frac{1}{2}}$).

We now introduce the "finite-volume shape functions" for the components of the velocity. Let us denote by $\mathcal{I}^x \subset \mathbb{N}^2$ (resp. $\mathcal{I}^y \subset \mathbb{N}^2$) the set of pairs (i,j) which are admissible in the sense that $\boldsymbol{x}_{i-\frac{1}{2},j}$ (resp. $\boldsymbol{x}_{i,j-\frac{1}{2}}$) is the mass center of a vertical (resp. horizontal) face of the mesh. For $(i,j) \in \mathcal{I}^x$, we denote by $\boldsymbol{\varphi}^{x,(i-\frac{1}{2},j)}$ the shape function associated to the degree of freedom of the x-component of the velocity located at $\boldsymbol{x}_{i-\frac{1}{2},j}$; this discrete function is defined by:

$$(\boldsymbol{\varphi}^{x,(i-\frac{1}{2},j)})^x_{k-\frac{1}{2},\ell} = \delta^i_k\ \delta^j_\ell,\ \forall (k,\ell) \in \mathcal{I}^x \text{ and } (\boldsymbol{\varphi}^{x,(i-\frac{1}{2},j)})^y_{k,\ell-\frac{1}{2}} = 0,\ \forall (k,\ell) \in \mathcal{I}^y.$$

Similarly, for $(i,j) \in \mathcal{I}^y$, we denote by $\boldsymbol{\varphi}^{y,(i,j-\frac{1}{2})}$ the shape function associated to the degree of freedom for the y-component of the velocity located at $\boldsymbol{x}_{i,j-\frac{1}{2}}$, which is defined by

$$(\boldsymbol{\varphi}^{y,(i,j-\frac{1}{2})})^x_{k-\frac{1}{2},\ell} = 0,\ \forall (k,\ell) \in \mathcal{I}^x \text{ and } (\boldsymbol{\varphi}^{y,(i,j-\frac{1}{2})})^y_{k,\ell-\frac{1}{2}} = \delta^i_k\ \delta^j_\ell,\ \forall (k,\ell) \in \mathcal{I}^y.$$

Then, the viscous diffusion and dissipation terms are defined by the following analogues of (3.13) and (3.14):

$$\begin{aligned} &\forall (i,j) \in \mathcal{I}^x, \qquad -(\mathrm{div}\boldsymbol{\tau}(\tilde{\boldsymbol{u}}))^x_{i-\frac{1}{2},j} = \frac{1}{|K^x_{i-\frac{1}{2},j}|}\int_\Omega \boldsymbol{\tau}^{\mathcal{M}}(\tilde{\boldsymbol{u}}) : \boldsymbol{\nabla}^{\mathcal{M}}\boldsymbol{\varphi}^{x,(i-\frac{1}{2},j)}\,\mathrm{d}\boldsymbol{x}, \\ &\forall (i,j) \in \mathcal{I}^y, \qquad -(\mathrm{div}\boldsymbol{\tau}(\tilde{\boldsymbol{u}}))^y_{i,j-\frac{1}{2}} = \frac{1}{|K^y_{i,j-\frac{1}{2}}|}\int_\Omega \boldsymbol{\tau}^{\mathcal{M}}(\tilde{\boldsymbol{u}}) : \boldsymbol{\nabla}^{\mathcal{M}}\boldsymbol{\varphi}^{y,(i,j-\frac{1}{2})}\,\mathrm{d}\boldsymbol{x}, \end{aligned} \tag{3.17}$$

and:

$$(\boldsymbol{\tau}(\tilde{\boldsymbol{u}}) : \boldsymbol{\nabla}\tilde{\boldsymbol{u}})_K = \frac{1}{|K|}\int_K \boldsymbol{\tau}^{\mathcal{M}}(\tilde{\boldsymbol{u}}) : \boldsymbol{\nabla}^{\mathcal{M}}\tilde{\boldsymbol{u}}\,\mathrm{d}\boldsymbol{x}. \tag{3.18}$$

As a consequence of these definitions, as announced, the constraints (3.11) and (3.12) are satisfied. Let us now check that the definition (3.17) coincides with the usual definition of the viscous diffusion term for the MAC scheme. To this purpose, we consider the equation corresponding to the $(i-\frac{1}{2},j)$ unknown for the x-component of the velocity. The shape function associated to this equation is $\boldsymbol{\varphi}^{x,(i-\frac{1}{2},j)}$ and its non-zero partial derivatives are $\partial^{\mathcal{M}}_x\boldsymbol{\varphi}^{x,(i-\frac{1}{2},j)}$ and $\partial^{\mathcal{M}}_y\boldsymbol{\varphi}^{x,(i-\frac{1}{2},j)}$:

$$\partial^{\mathcal{M}}_x\boldsymbol{\varphi}^{x,(i-\frac{1}{2},j)} = \left|\begin{array}{l} \dfrac{1}{h^x_{i-1}} \text{ over } K_{i-1,j}, \\ \dfrac{-1}{h^x_i} \text{ over } K_{i,j}, \\ 0 \text{ elsewhere,} \end{array}\right. \qquad \partial^{\mathcal{M}}_y\boldsymbol{\varphi}^{x,(i-\frac{1}{2},j)} = \left|\begin{array}{l} \dfrac{1}{h^y_{j-\frac{1}{2}}} \text{ over } K^{xy}_{i-\frac{1}{2},j-\frac{1}{2}}, \\ \dfrac{-1}{h^y_{j+\frac{1}{2}}} \text{ over } K^{xy}_{i-\frac{1}{2},j+\frac{1}{2}}, \\ 0 \text{ elsewhere.} \end{array}\right.$$

The corresponding entries of the discrete stress tensor of $\tilde{\boldsymbol{u}}$ (recall that, at the continuous level, this tensor is defined by $\boldsymbol{\tau}^{xx}(\tilde{u}) = \frac{4}{3}\,\mu\partial_x\tilde{u}^x - \frac{2}{3}\,\mu\partial_y\tilde{u}^y$ and $\boldsymbol{\tau}^{xy} = \mu(\partial_y\tilde{u}^x + \partial_x\tilde{u}^x)$) read over $K_{i-1+\varepsilon,j}$, with $\varepsilon = 0$ and $\varepsilon = 1$:

$$\boldsymbol{\tau}^{\mathcal{M}}(\tilde{\boldsymbol{u}})^{xx}_{i-1+\varepsilon,j} = \frac{4}{3}\,\mu_{i-1+\varepsilon,j}\frac{\tilde{u}^x_{i-\frac{1}{2}+\varepsilon,j} - \tilde{u}^x_{i-\frac{3}{2}+\varepsilon,j}}{h^x_{i-1+\varepsilon}} - \frac{2}{3}\,\mu_{i-1+\varepsilon,j}\frac{\tilde{u}^y_{i+\varepsilon,j+\frac{1}{2}} - \tilde{u}^y_{i+\varepsilon,j-\frac{1}{2}}}{h^y_j},$$

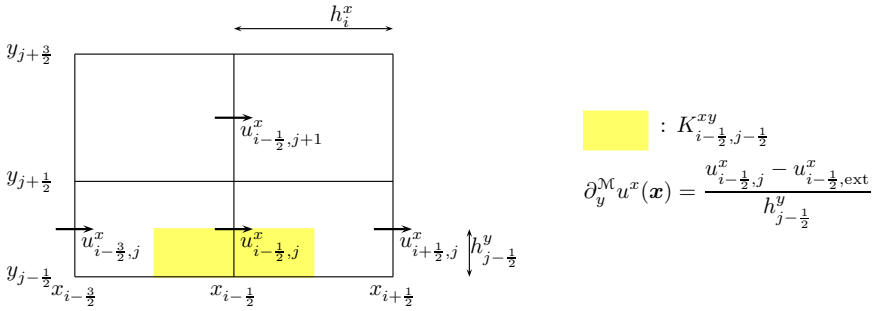

FIGURE 3.5. Boundary conditions, x-component of the velocity

and, over $K^{xy}_{i-\frac{1}{2},j-\frac{1}{2}+\varepsilon}$, still with $\varepsilon = 0$ and $\varepsilon = 1$:

$$\boldsymbol{\tau}^{\mathcal{M}}(\tilde{\boldsymbol{u}})^{xy}_{i-\frac{1}{2},j-\frac{1}{2}+\varepsilon} = \mu_{i-\frac{1}{2},j-\frac{1}{2}+\varepsilon}\Big[\frac{\tilde{u}^x_{i-\frac{1}{2},j+\varepsilon} - \tilde{u}^x_{i-\frac{1}{2},j-1+\varepsilon}}{h^y_{j-\frac{1}{2}+\varepsilon}} + \frac{\tilde{u}^y_{i-1,j-\frac{1}{2}+\varepsilon} - \tilde{u}^y_{i,j-\frac{1}{2}+\varepsilon}}{h^x_{i-\frac{1}{2}}}\Big].$$

We thus get:

$$\int_\Omega \boldsymbol{\tau}^{\mathcal{M}}(\tilde{\boldsymbol{u}})^{xx}\ \partial_x^{\mathcal{M}} \boldsymbol{\varphi}^{x,(i-\frac{1}{2},j)}\,\mathrm{d}\boldsymbol{x} = F_{i,j} - F_{i-1,j},$$

where, for $\varepsilon = 0$ and $\varepsilon = 1$, $F_{i-1+\varepsilon,j} = h^y_j\ \boldsymbol{\tau}^{\mathcal{M}}(\tilde{\boldsymbol{u}})^{xx}_{i-1+\varepsilon,j}$, which is the usual viscous diffusion flux across the face $\sigma^x_{i-1+\varepsilon,j}$ (see Figure 3.1). Similarly,

$$\int_\Omega \boldsymbol{\tau}^{\mathcal{M}}(\tilde{\boldsymbol{u}})^{xy}\ \partial_y^{\mathcal{M}} \boldsymbol{\varphi}^{x,(i-\frac{1}{2},j)}\,\mathrm{d}\boldsymbol{x} = F_{i-\frac{1}{2},j+\frac{1}{2}} - F_{i-\frac{1}{2},j-\frac{1}{2}},$$

where, for $\varepsilon = 0$ and $\varepsilon = 1$, $F_{i-\frac{1}{2},j-\frac{1}{2}+\varepsilon} = h^x_{i-1/2}\ \boldsymbol{\tau}^{\mathcal{M}}(\tilde{\boldsymbol{u}})^{xy}_{i-\frac{1}{2},j-\frac{1}{2}+\varepsilon}$, which is the usual expression of the MAC viscous flux across the face $\sigma^x_{i-\frac{1}{2},j-\frac{1}{2}+\varepsilon}$ (once again defined on Figure 3.1). The same arguments apply for the y-component of the momentum balance equation.

Let us now show how to extend these definitions up to the boundary and how to deal with Dirichlet boundary conditions. Modification of the above material is necessary only for the definition of a "twice-staggered cell" K^{xy} associated to a vertex lying on the boundary, and for one of the discrete partial derivatives on this cell: $\partial_y^{\mathcal{M}} u^x$ near an horizontal boundary and $\partial_x^{\mathcal{M}} u^y$ near a vertical boundary. Let us deal for instance with the first case, using the notations of Figure 3.5. Roughly speaking, everything is done as if we were supposing that there is an additional horizontal stripe of mesh at the boundary, with zero height and where the x-velocity is set at the prescribed value, let us say $u^x_{i-\frac{1}{2},\mathrm{ext}}$ (which is zero in case of homogeneous Dirichlet boundary conditions). Therefore, $K^{xy}_{i-\frac{1}{2},j-\frac{1}{2}} = (x_{i-1}, x_i) \times (y_{j-\frac{1}{2}}, y_j)$, $h^y_{j-\frac{1}{2}} = h^y_j/2$ and

$$\partial_y^{\mathcal{M}} u^x(\boldsymbol{x}) = \frac{u^x_{i-\frac{1}{2},j} - u^x_{i-\frac{1}{2},\mathrm{ext}}}{h^y_{j-\frac{1}{2}}}, \quad \forall \boldsymbol{x} \in K^{xy}_{i-\frac{1}{2},j-\frac{1}{2}}.$$

The other partial derivative $\partial_x^{\mathcal{M}} u^y$ defined on $K^{xy}_{i-\frac{1}{2},j-\frac{1}{2}}$ is computed with its usual expression, but using the prescribed value for $u^y_{i-1,j-\frac{1}{2}}$ and $u^y_{i,j-\frac{1}{2}}$; this derivative vanishes in case of homogeneous boundary conditions (in fact, as soon as the prescribed value for u^y does not depend on x). For the computation of the partial derivative of the shape functions, the external value is always zero (which

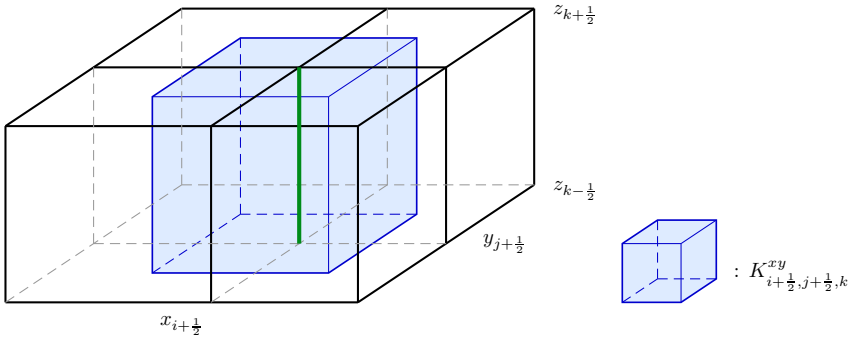

FIGURE 3.6. The xy-staggered cell $K^{xy}_{i+\frac{1}{2},j+\frac{1}{2},k}$, used in the definition of $\partial_y^{\mathcal{M}} u^x$, $\partial_x^{\mathcal{M}} u^y$, and $\boldsymbol{\tau}^{\mathcal{M}}(\boldsymbol{u})_{x,y} = \boldsymbol{\tau}^{\mathcal{M}}(\boldsymbol{u})_{y,x}$.

is consistent with the fact that a test function for an elliptic boundary value problem is supposed to vanish on the boundary).

Remark 3.2 (Neumann or perfect slip boundary conditions)**.** In the case of Neumann or perfect slip boundary condition, the quantity at the boundary is supposed to be the same as in the domain (*i.e.* , for the example chosen above, $u^x_{i-\frac{1}{2},\text{ext}} = u^x_{i-\frac{1}{2},j}$). If the considered Neumann boundary condition involves a non-zero shear surface force, this latter must be added at the righ-hand side of the balance equation.

The three-dimensional case – Extending the computations of the preceding section to three space dimensions yields the following construction.

- First, define three new meshes, which are "edge-centred": $K^{xy}_{i+\frac{1}{2},j+\frac{1}{2},k}$ is staggered from the primal mesh $K_{i,j,k}$ in the x and y direction (so $K^{xy}_{i+\frac{1}{2},j+\frac{1}{2},k} = (x_i, x_{i+1}) \times (y_i, y_{j+1}) \times (z_{k-\frac{1}{2}}, z_{k+\frac{1}{2}})$, see Figure 3.6), $K^{xz}_{i+\frac{1}{2},j,k+\frac{1}{2}}$ in the x and z direction, and $K^{yz}_{i,j+\frac{1}{2},k+\frac{1}{2}}$ in the y and z direction.
- The partial derivatives of the velocity components are then defined as piecewise constant functions, the value of which is obtained by natural finite differences:
  - for $\partial_x^{\mathcal{M}} u^x$, $\partial_y^{\mathcal{M}} u^y$ and $\partial_z^{\mathcal{M}} u^z$, on the primal mesh,
  - for $\partial_y^{\mathcal{M}} u^x$ and $\partial_x^{\mathcal{M}} u^y$ on the cells $(K^{xy}_{i+\frac{1}{2},j+\frac{1}{2},k})$,
  - for $\partial_z^{\mathcal{M}} u^x$ and $\partial_x^{\mathcal{M}} u^z$ on the cells $(K^{xz}_{i+\frac{1}{2},j,k+\frac{1}{2}})$,
  - for $\partial_y^{\mathcal{M}} u^z$ and $\partial_z^{\mathcal{M}} u^y$ on the cells $(K^{yz}_{i,j+\frac{1}{2},k+\frac{1}{2}})$.
- Then, define four families of values for the viscosity field, μ, μ^{xy}, μ^{xz} and μ^{yz}, associated to the primal and the three edge-centred meshes respectively.
- The shear stress tensor is obtained by the extension of (3.17) to $d = 3$, and the dissipation term is given by (3.18).

3.3. **The heat diffusion term**

The discretization of the diffusion term depends on whether the mesh is super-admissible (in the sense of Section 2, Condition (2.1)) or not. In the first case, we use the usual finite volume scheme based on

a two-point approximation of the fluxes [12]:

$$\forall K \in \mathcal{M}, \qquad -\lambda\ (\Delta e)_K = \lambda \sum_{\sigma=K|L\in\mathcal{E}(K)} \frac{|\sigma|}{d_\sigma}\ (e_K - e_L). \tag{3.19}$$

Note that, in this relation, no flux is computed on the external faces, which is consistent with homogeneous Neumann boundary conditions. In the second case, we use the so-called SUSHI scheme, in the variant described in [38, Section 3.1] for general meshes.

For $a \in \mathbb{R}$, let us denote by a^+ and a^- the positive and negative part of a respectively, *i.e.* $a^+ = \max(a, 0)$ and $a^- = -\min(a, 0)$, so $a^+ \geq 0$, $a^- \geq 0$ and $a = a^+ - a^-$. For the scheme to ensure the positivity of the internal energy, we need the Laplace operator to be monotone, in the following sense:

$$\forall\ (e_K)_{K\in\mathcal{M}} \subset \mathbb{R}, \qquad \sum_{K\in\mathcal{M}} -\lambda\ (\Delta e)_K\ (-e_K^-) \geq 0. \tag{3.20}$$

Lemma 3.3. *The finite volume scheme based on the two-point approximation of the fluxes* (3.19) *satisfies the property* (3.20)*.*

Proof. Let $(e_K)_{K\in\mathcal{M}} \subset \mathbb{R}$ be given. Then, by definition and then reordering the sums:

$$\begin{aligned}\sum_{K\in\mathcal{M}} -\lambda\ (\Delta e)_K\ (-e_K^-) &= \sum_{K\in\mathcal{M}} (-e_K^-) \sum_{\sigma=K|L\in\mathcal{E}(K)} \frac{|\sigma|}{d_\sigma}\ (e_K - e_L) \\ &= \sum_{\sigma=K|L\in\mathcal{E}_{\rm int}} \frac{|\sigma|}{d_\sigma}\ (e_K - e_L)\ (e_L^- - e_K^-),\end{aligned}$$

and the conclusion follows by remarking that the function $s \mapsto s^-$ is non-increasing. ∎

Remark 3.4 (Two-points flux discrete Laplace operator with Dirichlet boundary conditions)**.** In case of Dirichlet boundary conditions, the definition (3.19) of the discrete Laplace operator must be changed to:

$$-(\Delta e)_K = \sum_{\sigma=K|L\in\mathcal{E}(K)} \frac{|\sigma|}{d_\sigma}\ (e_K - e_L) + \sum_{\sigma\in\mathcal{E}(K)\cap\mathcal{E}_{\rm ext}} \frac{|\sigma|}{d_\sigma}\ (e_K - e_{\sigma,D}),$$

where $e_{\sigma,D}$ stands for the prescribed value for e on the face σ, and, for an external face, d_σ stands for the distance between σ and $\boldsymbol{x}_K$. Let us suppose that $e_{\sigma,D} \geq 0$. The additional terms (compared to the Neumann case) in the expression of $\sum_{K\in\mathcal{M}} -\lambda\ (\Delta e)_K\ (-e_K^-)$ read:

$$\lambda \sum_{\sigma\in\mathcal{E}_{\rm ext},\ \sigma\in\mathcal{E}(K)} \frac{|\sigma|}{d_\sigma}\ (e_K - e_{\sigma,D})(-e_K^-),$$

and this sum is non-negative, since, by definition of the negative part of a real number, both products $e_K\,(-e_K^-)$ and $-e_{\sigma,D}\,(-e_K^-)$ are non-negative. The two-point fluxes discrete Laplace operator thus still satisfies the assumption (3.20) in case of Dirichlet boundary conditions.

Unfortunately, the fact that the discrete Laplace operator obtained by the SUSCHI scheme satisfies (3.20) is wrong on general meshes; this restricts the applicability of the following analysis to super-admissible meshes or to the Euler equations. As a matter of fact, however, this seems unavoidable that the stability of the scheme be conditioned to the fact that internal energy remains non-negative, and thus that the diffusion operator is monotone; circumventing this problem will require to build a discrete Laplace operator satisfying a maximum principle, which is still an active subject of research (and, of course, out of the scope of the present paper).

4. Properties of the scheme

4.1. A priori estimates

The following lemma is an easy extension of [20, Lemma 3.11], to cope with diffusion terms (while [20] only deals with Euler equations). Its proof follows, at the discrete level, the computation performed in Appendix A, which clarifies the effects of the pressure gradient scaling step.

Lemma 4.1 (Discrete kinetic energy balance)**.**
A solution to the scheme (3.1) *satisfies the following equality, for* $1 \leq i \leq d$, $\sigma \in \mathcal{E}_{\rm S}^{(i)}$ *and* $0 \leq n \leq N-1$*:*

$$\frac{1}{2}\frac{|D_\sigma|}{\delta t}\Big[\rho^n_{D_\sigma}(u^{n+1}_{\sigma,i})^2 - \rho^{n-1}_{D_\sigma}(u^n_{\sigma,i})^2\Big] + \frac{1}{2}\sum_{\varepsilon\in\bar{\mathcal{E}}(D_\sigma)} F^n_{\sigma,\varepsilon}\ \tilde{u}^{n+1}_{\sigma,i}\ \tilde{u}^{n+1}_{\sigma',i}$$
$$+ |D_\sigma|\ \boldsymbol{\nabla}_{\sigma,i}(p^{n+1})\ u^{n+1}_{\sigma,i} - |D_\sigma|\,\mathrm{div}_{\sigma,i}\,\boldsymbol{\tau}(\tilde{\boldsymbol{u}}^{n+1})\ \tilde{u}^{n+1}_{\sigma,i} + P^{n+1}_{\sigma,i} - P^n_{\sigma,i} = -R^{n+1}_{\sigma,i}, \quad (4.1)$$

where

$$P^{n+1}_{\sigma,i} = \frac{\delta t\,|\sigma|^2}{2|D_\sigma|}\ \frac{1}{\rho^n_{D_\sigma}}\,(p^{n+1}_L - p^{n+1}_L)^2, \quad R^{n+1}_{\sigma,i} = \frac{1}{2}\ \frac{|D_\sigma|}{\delta t}\ \rho^{n-1}_{D_\sigma}\ (\tilde{u}^{n+1}_{\sigma,i} - u^n_{\sigma,i})^2. \quad (4.2)$$

The residual terms $R^{n+1}_{\sigma,i}$ may be seen as a numerical dissipation generated by the upwinding in time of the scheme (*i.e.* the use of a backward time discretization). For viscous flows, it may be anticipated that these terms tend to zero when the space and time steps tend to zero. On the opposite, it is not the case when dealing with Euler equations, where they may subsist as measures borne by the shocks (see Remark 4.2 below). Since, in this context, the scheme needs to be consistent with the total energy balance, this dissipation (as the usual physical viscous dissipation) has to be compensated in the internal energy balance; this is done by the corrective terms S_K in (3.1e), which we are now in position to define:

$$\forall K \in \mathcal{M},\ S^{n+1}_K = \sum_{i=1}^d S^{n+1}_{K,i},\ \text{with}\quad S^{n+1}_{K,i} = \frac{1}{2}\,\rho^{n-1}_K \sum_{\sigma\in\mathcal{E}(K)\cap\mathcal{E}_{\rm S}^{(i)}} \frac{|D_{K,\sigma}|}{\delta t}\ (\tilde{u}^{n+1}_{\sigma,i} - u^n_{\sigma,i})^2. \quad (4.3)$$

Thanks to the definition (3.4) of the density on the duals cells, this relation results from a distribution of the residual terms associated to a face to its (one or two) adjacent cells. Therefore, we get:

$$\sum_{K\in\mathcal{M}} S^{n+1}_K = \sum_{i=1}^d \sum_{\sigma\in\mathcal{E}_{\rm S}^{(i)}} R^{n+1}_{\sigma,i}. \quad (4.4)$$

A theoretical justification of this process is provided in [20], where it is shown in the 1D case that, if the scheme is stable and converges to a limit, this limit indeed satisfies the weak form of the total energy balance (1.1c). Note however that the scheme does not provide a conservative discretization of the (conservative) total energy balance. Indeed, the discrete kinetic energy balance(s) and the internal energy balance are not posed on the same mesh: precisely speaking, the kinetic energy is the sum of the terms $\frac{1}{2}\rho u_i^2$, for $1 \leq i \leq d$, and the discrete balance equation (4.1) for each of these terms is posed on the mesh associated to the i^{th} velocity component (that is d different meshes for the MAC scheme, and a single mesh for the RT-CR discretization), while the internal energy balance is posed on the primal mesh. To the best of our knowledge, these $d+1$ relations cannot be combined to obtain a consistent discrete analogue of the total energy balance. This latter equation is only obtained in the weak sense at the limit of vanishing time and space steps. A similar algorithm was developed for co-located discretization in [23], in which case the discrete kinetic energy inequality and internal energy equation are written on the same mesh, so that local conservation of the total energy can be

ensured. Note that for both types of discretizations (staggered or colocated), without corrective terms, the scheme is observed in numerical experiments to yield wrong shock solutions, which do not satisfy the Rankine-Hugoniot conditions.

Remark 4.2 (Behaviour of the remainder R (or the corrective term S))**.** Let us consider a one-dimensional problem posed over $\Omega = (0,1)$ and $t \in (0,1)$, and let u be a discrete function increasing with x and such that, for $x \in (0,1)$, $u(x,t) = 0$ for $t \in (0, T_0(x))$, $u(x,t) = 1$ for $t \in (T_1(x), 1)$ and $u(x,.)$ affine in the interval $(T_0(x), T_1(x))$. We suppose in addition that the number of time steps in the interval $(T_0(x), T_1(x))$ does not depend on x, and is equal to N. This situation is obtained, for instance, when u is a travelling-in-time piecewise-affine profile (with $T_0(x) = x_0 + c\,t$ and $T_1(x) = x_1 + c\,t$, c being the travelling velocity). In these conditions, for $\sigma \in \mathcal{E}$, the difference $u_\sigma^{n+1} - u_\sigma^n$ is, up to side effects, equal to $1/N$ for N time steps and to zero for the other ones, so we get, for the space-time L^1-norm of R or S:

$$\sum_{n=0}^{N-1} \sum_{\sigma \in \mathcal{E}} \delta t \; R_\sigma^{n+1} = \sum_{n=0}^{N-1} \sum_{K \in \mathcal{M}} \delta t \; S_K^{n+1} \sim |\Omega| \; N \; \frac{1}{N^2} = \frac{|\Omega|}{N}.$$

Let us now make this computation for a sequence of more and more refined meshes. We then have two situations: either N is bounded, and the L^1-norm of R or S does not vanish, or N tends to $+\infty$ when h tends to zero. These two situations seem to be encountered in the computations [20]:

- Shocks appear to be captured in a finite number of cells, for any space step, and so, when h tends to zero, R and S tend to measures borne by the shocks (the L^1-norm remains constant while the measure of the support tends to zero); consequently, for solutions combining only shocks, one may expect a near-to-one order of convergence in L^1-norm. This behaviour may be explained by the fact that the flow is compressive, and the convection counterbalances the numerical diffusion.

- On the contrary, the scheme is much more diffusive at contact discontinuities; if we suppose a diffusion induced by the upwinding, with a velocity which remains constant at the contact discontinuity (so the diffusion is also constant, and of range h), we may anticipate a smearing of the solution jump over a distance scaling like $h^{1/2}$. In this case, R and S tend to zero. Moreover, the first order convergence is lost: the order is reduced to approximately $1/2$ (still in L^1-norm) in numerical experiments.

We now turn to the positivity of the scalar variables. The positivity of the density is a consequence of the upwind discretization of the mass balance equation [14, Lemma 2.1]. To prove that the internal energy remains positive, we need a preliminary lemma, which we now state. Let ψ a regular real function. Then, at the continuous level, the following computation holds (formally), using twice the mass balance equation:

$$\begin{aligned}\psi'(e)\left(\partial_t(\rho e) + \operatorname{div}(\rho e \boldsymbol{u})\right) &= \rho\psi'(e)\left(\partial_t e + \boldsymbol{u}\cdot\boldsymbol{\nabla} e\right)\\ &= \rho\Big(\partial_t(\psi(e)) + \boldsymbol{u}\cdot\boldsymbol{\nabla}(\psi(e))\Big) = \partial_t(\rho\psi(e)) + \operatorname{div}(\rho\psi(e)\boldsymbol{u}).\end{aligned}$$

Thus, integrating over the domain Ω and using the boundary conditions:

$$\int_\Omega \psi'(e)\left(\partial_t(\rho e) + \operatorname{div}(\rho e\boldsymbol{u})\right)\mathrm{d}\boldsymbol{x} = \frac{d}{dt}\int_\Omega \rho\psi(e)\,\mathrm{d}\boldsymbol{x}.$$

The following lemma states a discrete analogue of this identity, which holds only for convex functions ψ, because of the diffusion generated by the upwinding of the convection term. Its proofs is a straightforward consequence of [20, Lemma A.2],

Lemma 4.3. *Let ψ, $\mathbb{R} \longrightarrow \mathbb{R}$, be a continuously differentiable convex function. A solution to the scheme* (3.1) *satisfies the following inequality:*

$$\sum_{K\in\mathcal{M}} |K|\ \psi'(e_K^{n+1})\Big[\frac{1}{\delta t}\left(\rho_K^{n+1}e_K^{n+1}-\rho_K^n e_K^n\right)+\mathrm{div}_K(\rho^{n+1}e^{n+1}\boldsymbol{u}^{n+1})\Big] \geq \frac{1}{2}\sum_{K\in\mathcal{M}}\frac{|K|}{\delta t}\ \Big[\rho_K^{n+1}\,\psi(e_K^{n+1})-\rho_K^n\,\psi(e_K^n)\Big]. \quad (4.5)$$

We are now in position to state and prove the following result.

Lemma 4.4 (Positivity of the internal energy)**.** *Let us suppose that the discrete heat diffusion operator satisfies the monotonicity property* (3.20)*, and that the equation of state satisfies* (1.8)*. Let n be such that $0 \leq n \leq N-1$, and let us suppose that $e^n > 0$ (i.e. $e_K^n > 0, \forall K \in \mathcal{M}$). Then a solution to the scheme* (3.1) *satisfies $e^{n+1} > 0$.*

Proof. Let us multiply the discrete internal energy equation (3.1e) by $-|K|\ (e_K^{n+1})^-$ and sum over $K \in \mathcal{M}$. We obtain $T_1 + T_2 + T_3 = T_4$ with:

$$T_1 = \sum_{K\in\mathcal{M}} -|K|\ (e_K^{n+1})^-\Big[\frac{1}{\delta t}\left(\rho_K^{n+1}e_K^{n+1}-\rho_K^n e_K^n\right)+\mathrm{div}_K(\rho^{n+1}e^{n+1}\boldsymbol{u}^{n+1})\Big],$$

$$T_2 = \sum_{K\in\mathcal{M}} -|K|\ (e_K^{n+1})^-\,p_K^{n+1}\,\mathrm{div}_K(\boldsymbol{u}^{n+1}),$$

$$T_3 = \sum_{K\in\mathcal{M}} \lambda\,|K|\ (e_K^{n+1})^-\,(\Delta e^{n+1})_K,$$

$$T_4 = \sum_{K\in\mathcal{M}} -|K|\ (e_K^{n+1})^-\Big[\left(\boldsymbol{\tau}(\tilde{\boldsymbol{u}}^{n+1}):\boldsymbol{\nabla}\tilde{\boldsymbol{u}}^{n+1}\right)_K + S_K^{n+1}\Big].$$

Thanks to Lemma 4.3 applied with the continuously differentiable convex function $\psi(s) = (s^-)^2/2$, we have for the term T_1, since $e^n \geq 0$:

$$T_1 \geq \frac{1}{2}\sum_{K\in\mathcal{M}}\frac{|K|}{\delta t}\ \Big[\rho_K^{n+1}\left((e_K^{n+1})^-\right)^2-\rho_K^n\left((e_K^n)^-\right)^2\Big] = \frac{1}{2}\sum_{K\in\mathcal{M}}\frac{|K|}{\delta t}\rho_K^{n+1}\left((e_K^{n+1})^-\right)^2.$$

Thanks to Assumption (1.8), we have $T_2 = 0$, since, when $(e_K^{n+1})^- \neq 0$, $e_K^{n+1} \leq 0$ and so the pressure satisfies $p_K^{n+1} = \wp(\rho_K^{n+1}, e_K^{n+1}) = 0$. The relation (3.20) yields $T_3 \geq 0$. Finally, by construction, the viscous dissipation term and S_K^{n+1} are non-negative, so $T_4 \leq 0$. Gathering all the terms, we obtain:

$$\sum_{K\in\mathcal{M}}\frac{|K|}{\delta t}\rho_K^{n+1}\left((e_K^{n+1})^-\right)^2 \leq 0,$$

which shows that $(e_K^{n+1})^- = 0$, for all $K \in \mathcal{M}$, and thus $e^{n+1} \geq 0$. Let us now consider a cell K such that $e_K^{n+1} = 0$. The internal energy balance on K reads:

$$-\frac{1}{\delta t}\rho_K^n e_K^n - \sum_{\sigma=K|L}(F_{K,\sigma})^- e_L^{n+1} - \lambda\sum_{\sigma=K|L}\frac{|\sigma|}{d_\sigma}e_L^{n+1} = \Big(\boldsymbol{\tau}(\tilde{\boldsymbol{u}}^{n+1}):\boldsymbol{\nabla}\tilde{\boldsymbol{u}}^{n+1}\Big)_K + S_K^{n+1}.$$

The first term at the left-hand side is by assumption negative, the other terms are non-positive and the right-hand side is non-negative, which raises a contradiction. This concludes the proof. ∎

Finally, we obtain the following estimate, which is a discrete analogue of the conservation of the total energy.

Theorem 4.5 (Unconditional stability of the scheme)**.** *Let us suppose that the discrete heat diffusion operator satisfies the monotonicity property* (3.20)*, that the equation of state satisfies* (1.8)*, and that the initial conditions for ρ and e are positive. Then, for $0 \leq n \leq N-1$, a solution to the scheme* (3.1) *satisfies $\rho^{n+1} > 0$, $e^{n+1} > 0$ and the following estimate:*

$$\sum_{K\in\mathcal{M}} |K|\ \rho_K^{n+1} e_K^{n+1} + \frac{1}{2}\sum_{i=1}^{d}\sum_{\sigma\in\mathcal{E}_S^{(i)}} |D_\sigma|\ \rho_{D_\sigma}^{n}\ (u_{\sigma,i}^{n+1})^2 + \frac{\delta t^2}{2}\ |p^{n+1}|^2_{\rho^n,\mathcal{M}}$$

$$\leq \sum_{K\in\mathcal{M}} |K|\ \rho_K^{n} e_K^{n} + \frac{1}{2}\sum_{i=1}^{d}\sum_{\sigma\in\mathcal{E}_S^{(i)}} |D_\sigma|\ \rho_{D_\sigma}^{n-1}\ (u_{\sigma,i}^{n})^2 + \frac{\delta t^2}{2}\ |p^{n}|^2_{\rho^{n-1},\mathcal{M}} \quad (4.6)$$

where, for any discrete pressure q and density ρ,

$$|q|^2_{\rho,\mathcal{M}} = \sum_{\sigma=K|L\in\mathcal{E}_{\rm int}} \frac{1}{\rho_{D_\sigma}}\ \frac{|\sigma|^2}{|D_\sigma|}\ (q_L - q_K)^2.$$

Proof. Since the initial condition for ρ and e are assumed to be positive, by induction, the positivity of the density is ensured by the upwind discretization of the scheme, and the positivity of the internal energy follows from Lemma 4.4. Summing the discrete internal energy equation (3.1e) over the cells $K \in \mathcal{M}$, we obtain, by conservativity of the diffusion fluxes:

$$\sum_{K\in\mathcal{M}} \frac{|K|}{\delta t}\ [\rho_K^{n+1}\, e_K^{n+1} - \rho_K^n\, e_K^n] + \sum_{K\in\mathcal{M}} |K|\ p_K^{n+1}\ {\rm div}_K(\boldsymbol{u}^{n+1})$$

$$= \sum_{K\in\mathcal{M}} |K|\ (\boldsymbol{\tau}(\tilde{u}^{n+1}) : \boldsymbol{\nabla}\tilde{\boldsymbol{u}}^{n+1})_K + S_K^{n+1}.$$

On the other hand, summing over the edges and the components i the equation of discrete kinetic energy balance (4.1) yields, by conservativity of the convection flux of the kinetic energy:

$$\frac{1}{2}\sum_{i=1}^{d}\sum_{\sigma\in\mathcal{E}_S^{(i)}} \Big[\frac{|D_\sigma|}{\delta t}\Big(\rho_{D_\sigma}^n (u_{\sigma,i}^{n+1})^2 - \rho_{D_\sigma}^{n-1}(u_{\sigma,i}^n)^2\Big) + |D_\sigma|\ \boldsymbol{\nabla}_{\sigma,i}(p^{n+1})\ u_{\sigma,i}^{n+1} + P_{\sigma,i}^{n+1} - P_{\sigma,i}^n\Big]$$

$$= \sum_{i=1}^{d}\sum_{\sigma\in\mathcal{E}_S^{(i)}} \Big[|D_\sigma|\,{\rm div}_{\sigma,i}\,\boldsymbol{\tau}(\tilde{\boldsymbol{u}}^{n+1})\ \tilde{u}_{\sigma,i}^{n+1} - R_{\sigma,i}^{n+1}\Big].$$

Summing these two relations and using the $\boldsymbol{\nabla}$ − div duality property (3.9), the consistency property (3.12) of the viscous diffusion and dissipation terms, the fact that the residual term in the kinetic energy balance and the corrective term in the internal energy equation are designed to compensate themselves (Equation (4.4)) and the definition (4.2) of $P_{\sigma,i}^{n+1}$ concludes the proof. ∎

4.2. **Existence of a discrete solution**

We recall the following theorem, which is a consequence of the topological degree theory (see *e.g.* [11]), and which is a very powerful tool for the proof of existence of a solution to non-linear systems arising from the discretization of non-linear partial differential equations.

Theorem 4.6 (Application of the topological degree, finite dimensional case)**.**
Let V be a finite dimensional vector space on $\mathbb{R}$, $\|.\|$ a norm on V, let f be a continuous function

from V to V and let $R > 0$. Let us assume that there exists a continuous function $\mathcal{F} : V \times [0,1] \to V$ satisfying:

(i) $\mathcal{F}(.,1) = f$,

(ii) $\forall \alpha \in [0,1]$, *if $v \in V$ is such that $\mathcal{F}(v,\alpha) = 0$ then $v \in B_R = \{v \in V\ ; \|v\| < R\}$,*

(iii) *the topological degree of $\mathcal{F}(.,0)$ with respect to 0 and to B_R is equal to $d_0 \neq 0$.*

Then the topological degree of $\mathcal{F}(.,1)$ with respect to 0 and to B_R is also equal to $d_0 \neq 0$; consequently, there exists at least a solution $v \in B_R$ such that $f(v) = 0$.

Theorem 4.7. *Under the assumptions of Theorem 4.5, there exists a solution to the scheme* (3.1).

Proof. Let us begin with the velocity prediction step. The step is a linear system of unknown $\tilde{\boldsymbol{u}}$ and, applying Lemma 4.3 with $\psi(s) = s^2$ to each component of the velocity yields:

$$\frac{1}{2}\sum_{i=1}^{d}\sum_{\sigma\in\mathcal{E}_{\rm S}^{(i)}}\Big[\frac{|D_\sigma|}{\delta t}\ \rho_{D_\sigma}^n(\tilde{u}_{\sigma,i}^{n+1})^2 - |D_\sigma|\ \mathrm{div}_{\sigma,i}\,\boldsymbol{\tau}(\tilde{\boldsymbol{u}}^{n+1})\ \tilde{u}_{\sigma,i}^{n+1}\Big]$$

$$\leq \sum_{i=1}^{d}\sum_{\sigma\in\mathcal{E}_{\rm S}^{(i)}}\Big[|D_\sigma|\ \rho_{D_\sigma}^{n-1}(u_{\sigma,i}^n)^2 - |D_\sigma|\ \overline{\boldsymbol{\nabla}}_{\sigma,i}(p^{n+1})\ \tilde{u}_{\sigma,i}^{n+1}.\Big]$$

Since $\rho^n > 0$ and the sum associated to the viscous diffusion (which is equal, by construction, to the integral of the viscous dissipation over the domain) is non-negative, this relation yields an estimate for $\tilde{\boldsymbol{u}}^{n+1}$ by the Young's inequality. The system thus has one and only one solution.

Let us now define $M \in \mathbb{N}$ and $X \in \mathbb{R}^M$ by:

$$M = \sum_{i=1}^{d}\mathrm{card}(\mathcal{E}_{\rm S}^{(i)}) + 2\ \mathrm{card}(\mathcal{M}),\ X = \big((u_{\sigma,i}^{n+1})_{\sigma\in\mathcal{E}_{\rm S}^{(i)},\,1\leq i\leq d},\ (\rho_K^{n+1})_{K\in\mathcal{M}},\ (\rho_K^{n+1}e_K^{n+1})_{K\in\mathcal{M}}\big).$$

Let $\mathcal{F}$, $\mathbb{R}^M \times [0,1] \longrightarrow \mathbb{R}^M$ be the continuous function defined by

$$\mathcal{F}(X,\alpha) = \big((\mathcal{F}_{\sigma,i}^u)_{\sigma\in\mathcal{E}_{\rm S}^{(i)},\,1\leq i\leq d},\ (\mathcal{F}_K^\rho)_{K\in\mathcal{M}},\ (\mathcal{F}_K^e)_{K\in\mathcal{M}}\big)$$

with:

$$\forall\sigma\in\mathcal{E}_{\rm S}^{(i)},\ 1\leq i\leq d,\qquad \mathcal{F}_{\sigma,i}^u = \frac{1}{\delta t}\ \rho_{D_\sigma}^n\ (u_{\sigma,i}^{n+1} - \tilde{u}_{\sigma,i}^{n+1}) + \alpha\ \boldsymbol{\nabla}_{\sigma,i}(p^{n+1}) - \overline{\boldsymbol{\nabla}}_{\sigma,i}(p^{n+1}),$$

$$\forall K\in\mathcal{M},\qquad \mathcal{F}_K^\rho = \frac{1}{\delta t}(\rho_K^{n+1} - \rho_K^n) + \alpha\ \mathrm{div}_K(\rho^{n+1}\boldsymbol{u}^{n+1}),$$

$$\forall K\in\mathcal{M},\qquad \mathcal{F}_K^e = \frac{1}{\delta t}(\rho_K^{n+1}e_K^{n+1} - \rho_K^n e_K^n) - \Big(\boldsymbol{\tau}(\tilde{\boldsymbol{u}}^{n+1}) : \boldsymbol{\nabla}\tilde{\boldsymbol{u}}^{n+1}\Big)_K - S_K^{n+1}$$
$$+\alpha\ \Big[\mathrm{div}_K(\rho^{n+1}e^{n+1}\boldsymbol{u}^{n+1}) + p_K^{n+1}\ \mathrm{div}_K(\boldsymbol{u}^{n+1}) - \lambda\ (\Delta e^{n+1})_K\Big],$$

where, $\forall K\in\mathcal{M}$, $p_K^{n+1} = \wp(\rho_K^{n+1}, e_K^{n+1})$. The system of equations $\mathcal{F}(X,1) = 0$ corresponds to the correction step. The function $X \mapsto \mathcal{F}(X,0)$ is linear (note that ρ^n, $\tilde{\boldsymbol{u}}^{n+1}$, $\overline{\boldsymbol{\nabla}}(p^{n+1})$ and S^{n+1} are known quantities) and one to one. In addition, the positivity of ρ^{n+1} and e^{n+1} solution to $\mathcal{F}(X,\alpha) = 0$ is preserved for $\alpha \in [0,1]$, by the same arguments as for the scheme itself. By conservativity, the equation:

$$\sum_{K\in\mathcal{M}}\mathcal{F}_K^\rho = 0$$

yields a uniform (with respect to α) bound for ρ^{n+1} (in any norm, since we are in finite dimensions). Let us now consider the equation:

$$\sum_{i=1}^{d} \sum_{\sigma \in \mathcal{E}_S^{(i)}} \mathcal{F}_{\sigma,i}^{u}\, u_{\sigma,i}^{n+1} + \sum_{K \in \mathcal{M}} \mathcal{F}_K^{e} = 0.$$

Invoking the identity $2a(a-b) = a^2 + (a-b)^2 + b^2$, the $\boldsymbol{\nabla}$-div duality argument and, finally, the conservativity of the diffusion and convection fluxes of the internal energy, we obtain:

$$\frac{1}{2\delta t} \sum_{i=1}^{d} \sum_{\sigma \in \mathcal{E}_S^{(i)}} \rho_{D_\sigma}^{n}\, (u_{\sigma,i}^{n+1})^2 + \sum_{K \in \mathcal{M}} \rho_K^{n+1}\, e_K^{n+1} \leq C,$$

where the bound C only depends on known quantities (and is independent on α). We thus get a uniform bound for $\tilde{\boldsymbol{u}}^{n+1}$, $(\rho e)^{n+1}$ and, since ρ^{n+1} is controlled, on X. Hence Theorem 4.6 applies, and the correction step admits at least one solution. This concludes the proof. ∎

5. **Numerical tests**

We present in this section numerical tests, to assess the behaviour of the scheme. We begin with a convergence study, on a two-dimensional analytical solution (Section 5.1). Then we address the limiting cases which the scheme should be able to cope with, namely the computation of high speed inviscid flows and of low Mach number viscous flows. Consequently, sections 5.2, 5.3 and 5.4 are dedicated to classical benchmarks for Euler solvers, while we compute in the first part of Section 5.5 an (almost) incompressible flow around a cylinder. Since the three first Euler tests are performed with the MAC space discretization, we continue this study in the remaining of Section 5.5 by computing a high speed viscous flow on a general geometry (with the Rannacher-Turek space discretization), obtained by keeping the same domain as in the previous incompressible case and decreasing the pressure range (and thus the range of the speed of sound) up to get a supersonic flow. Finally, we address a three dimensional inviscid case in Section 5.6.

For all the following test-cases, the fluid is supposed to obey the equation of state:

$$p = (\gamma - 1)\, \rho\, e, \qquad \text{with } \gamma = 1.4.$$

Computations are performed with the software component library CALIF^{3}S, developed at IRSN [3].

5.1. **A convergence study**

In this section, we compare the numerical results obtained by implementing the above algorithm in CALIF^{3}S with an analytical solution. This latter is built as follows: we first derive an exact analytical solution to stationary Euler equations, by extending to compressible flows the classical test for incompressible flows often referred to as the "standing-vortex" problem; then the diffusion in the momentum balance equation and in the energy balance, and the viscous dissipation in this latter equation are dealt with by a compensation at the right-hand side; finally, the problem is made unstationary by a time translation (*i.e.* , given a constant vector field $\boldsymbol{a}$, the density ρ, the internal energy e and the velocity $\boldsymbol{v}$ are deduced from the steady state solution $\hat{\rho}$, $\hat{e}$ and $\hat{\boldsymbol{v}}$ by $\rho(\boldsymbol{x},t) = \hat{\rho}(\boldsymbol{x} - \boldsymbol{a}t)$, $e(\boldsymbol{x},t) = \hat{e}(\boldsymbol{x} - \boldsymbol{a}t)$ and $\boldsymbol{v}(\boldsymbol{x},t) = \hat{\boldsymbol{v}}(\boldsymbol{x} - \boldsymbol{a}t) + \boldsymbol{a}$; the change of variable $\boldsymbol{x} = \hat{\boldsymbol{x}} - \boldsymbol{a}t$ is also performed on the right hand sides).

By construction, the velocity field is divergence-free, without consequence on the convergence study (this specificity is not seen by the scheme whose solution is not discretely divergence-free); in addition, letting the sound speed tend to infinity (*i.e.* the Mach number tend to zero), we obtain a problem

which tends to an incompressible flow problem. This allows us to check the behaviour of the scheme in the zero Mach number limit. We therefore address four problems: Euler or Navier-Stokes equations, for a Mach number in the range of unity and in the range of 10^{-3}.

Steady solution to the Euler equations – As in the standing-vortex problem, we search for a velocity perpendicular to the position vector $\boldsymbol{x} = (x, y)$, with a magnitude only depending on the radius:

$$\boldsymbol{u}(\boldsymbol{x}) = \begin{bmatrix} u_1 \\ u_2 \end{bmatrix} = f(\xi) \begin{bmatrix} -y \\ x \end{bmatrix},$$

where $\xi = |\boldsymbol{x}|^2 = (x^2 + y^2)^2$. Since this velocity field is divergence-free, we have, for $i = 1,\ 2$,

$$\mathrm{div}(\rho u_i \boldsymbol{u}) = \boldsymbol{u} \cdot \boldsymbol{\nabla}(\rho u_i) = \rho \boldsymbol{u} \cdot \boldsymbol{\nabla} u_i + u_i \boldsymbol{u} \cdot \boldsymbol{\nabla}\rho.$$

Choosing $\rho = \varrho(\xi)$, we observe that

$$\mathrm{div}(\rho \boldsymbol{u}) = \boldsymbol{u} \cdot \boldsymbol{\nabla}\rho = 0,$$

and the mass balance equation is thus satisfied. In addition, $\mathrm{div}(\rho u_i \boldsymbol{u}) = \rho \boldsymbol{u} \cdot \boldsymbol{\nabla} u_i$, and an easy computation yields:

$$\rho \begin{bmatrix} \boldsymbol{u} \cdot \boldsymbol{\nabla} u_1 \\ \boldsymbol{u} \cdot \boldsymbol{\nabla} u_2 \end{bmatrix} = -\varrho(\xi)\ f(\xi)^2 \begin{bmatrix} x \\ y \end{bmatrix}$$

Let us now suppose that the pressure reads $p = g(\xi)$. We thus have:

$$\boldsymbol{\nabla} p = 2g'(\xi) \begin{bmatrix} x \\ y \end{bmatrix}.$$

The momentum balance equation is therefore satisfied provided that

$$g' = \frac{1}{2}\rho f^2,\ \text{so } g(\xi) = p_0 + \frac{1}{2}\int_0^\xi \varrho(s)\, f(s)^2\, \mathrm{d}s,$$

with p_0 a given pressure. Finally, the equation of state yields $e = p/((\gamma - 1)\rho)$, thus e is a function of ξ only, and we have:

$$\mathrm{div}(\rho e \boldsymbol{u}) + p\, \mathrm{div}\boldsymbol{u} = \boldsymbol{u} \cdot \boldsymbol{\nabla}(\rho e) + p\, \mathrm{div}\boldsymbol{u},$$

and both terms vanish since $\boldsymbol{\nabla}(\rho e)$ is normal to $\boldsymbol{u}$ and $\mathrm{div}\boldsymbol{u} = 0$, which shows that the energy balance is satisfied.

Numerical tests – We choose for f and ϱ the following functions:

$$f(\xi) = \left| \begin{array}{l} 40\ \xi^2 (1 - \xi)^2 \text{ if } \xi \leq 1 \\ 0 \text{ otherwise} \end{array} \right. , \qquad \varrho = 1 + f,$$

so the vortex is local (*i.e.* of finite spatial extension) and both functions are in $\mathrm{H}^2(\Omega)$. The center of the vortex is initially located at $\boldsymbol{x}_0 = (0, 0)^t$, the translation velocity $\boldsymbol{a}$ is set to $\boldsymbol{a} = (1, 1)^t$ and $\Omega = (-1.5,\ 2.5)^2$. The range of variation of each unknown is $\rho \in [1,\ 3.5]$, $v_i \in [-0.8,\ 2.8]$ for $i = 1, 2$ and $p \in [p_0,\ p_0 + 3.93]$. The final time is $t = 1$, and the solution is constant over the boundary all over the computational interval, and thus may be fixed to this value if the diffusion is taken into account (for the Euler equations, the normal velocity is set to zero, and so are all the convection fluxes; since the pressure gradient operator is built as the transposed of the divergence, it vanishes on the boundaries). The considered meshes are $n \times n$ grids, with $n \in \{80,\ 160,\ 320,\ 640,\ 1280\}$, and the time step is $\delta t = 0.01 \times 80/n$, so the CFL number is constant, and close to 2 (with a CFL number related to the material velocity only, defined by CFL$=(\rho|\boldsymbol{u}|\ \delta t)/h$). The space discretization is performed with the MAC scheme.

Two tests are performed or the full Navier-Stokes equations with diffusion coefficients equal to $\mu = 0.1$ and $\lambda = 0.1\,\gamma$: in the first one, $p_0 = 10$, so the celerity of sound waves is close to 4 and

the maximum Mach number is close to 0.75; in the second one, $p_0 = 10^5$, so the Mach number is everywhere lower than 0.01.

Then we turn to the Euler equations, still with $p_0 = 10$ and $p_0 = 10^5$. For these two tests, a numerical viscosity μ_h is added to compensate the fact that we use a centered discretization in the convection term of the momentum balance equation. The quantity μ_h scales as the space step and is taken equal to $\mu = 0.01 * 80/n$, so close to $(\rho|\boldsymbol{u}|)_{\max} h/50$ where $(\rho|\boldsymbol{u}|)_{\max}$ stands for the maximum value of the quantity $\rho|\boldsymbol{u}|$; this value has to be compared with the range of the numerical viscosity which would be induced by an upwind discretization, which reads $\rho|\boldsymbol{u}|h/2$. Since this diffusion is a numerical artefact, no compensating term is added at the right hand side of the momentum and energy balance (contrary to what is done in the Navier-Stokes case). The transport of the internal energy is performed with an upwind discretization, so no stabilization has to be added (*i.e.* $\lambda = 0$).

On Figure 5.1, we plot the difference between the computed and the analytical solution at $t = 1$, as a function of the time and space step. This difference is evaluated in discrete L^2-norm, defined for both a regular and a discrete function ξ by:

$$||\xi|| = \Big(\sum_{K \in \mathcal{M}} |K| \ \xi(\boldsymbol{x}_K)^2 \Big)^{1/2},$$

where, for $K \in \mathcal{M}$, $\boldsymbol{x}_K$ stands for the mass center of K. There errors are normalized with respect to the error found for $n = 80$. We observe a very similar convergence for the two considered values of the Mach number, both in the Navier-Stokes and Euler case. For diffusive cases, the order of convergence is close to one; it is slightly lower (close to 0.8) without diffusion.

5.2. **The Mach 3 facing step**

We begin with a classical benchmark popularized in [48]. The computational domain is $\Omega = \overline{\Omega} \setminus \mathcal{S}$, where $\overline{\Omega} = (0,\, 3) \times (0,\, 1)$ and $\mathcal{S} = (0.6,\, 3) \times (0,\, 0.2)$, and the computation time interval is $(0,\, 0.25)$. The flow enters the domain through the left boundary $\{0\} \times (0, 1)$ with a velocity corresponding to Mach= 3:

$$\begin{bmatrix} \rho \\ \boldsymbol{u} \\ p \end{bmatrix} ((0, x_2)^t, t) = \begin{bmatrix} 1.4 \\ (3, 0)^t \\ 1 \end{bmatrix}, \qquad \forall x_2 \in (0, 1),\ \forall t \in (0, 0.25).$$

The initial data is the same as the inflow conditions:

$$\begin{bmatrix} \rho \\ \boldsymbol{u} \\ p \end{bmatrix} (\boldsymbol{x}, 0) = \begin{bmatrix} 1.4 \\ (3, 0)^t \\ 1 \end{bmatrix}, \qquad \forall \boldsymbol{x} \in \Omega.$$

At the right boundary $\{3\} \times (0, 1)$, the flow should be free, since it leaves the domain at a velocity greater than the sound speed. However, at the discrete level, an external pressure p_{ext} is needed to evaluate the pressure gradient on the boundary faces; it is taken here at the same value as the pressure at the entrance of the domain, so $p_{\text{ext}} = 1$; we discuss later on the effects of this numerical artefact. An impermeability and perfect slip condition (*i.e.* $\boldsymbol{u} \cdot \boldsymbol{n} = 0$, with $\boldsymbol{n}$ the unit outward normal on $\partial\Omega$, and $\boldsymbol{\tau}(\boldsymbol{n}) \cdot \boldsymbol{t} = 0$ for any vector $\boldsymbol{t}$ such that $\boldsymbol{t} \cdot \boldsymbol{n} = 0$) is prescribed on the rest of the boundary. At $t = 0$, a shock is generated by this boundary condition at the flow-facing step, and then moves upflow, and reaches and reflects on the upper and lower horizontal boundaries of the domain.

We display on Figure 5.2 the results obtained with the MAC space discretization, with a mesh built from a 1200×400 uniform grid, by removing the cells included in $\mathcal{S}$. The time step is $\delta t = h/4 = 0.001$, which corresponds to a CFL number in the range of unity with respect to the celerity of the fastest wave ($u_1 + c = 4$ at the inlet boundary, where c stands for the speed of sound). The artificial viscosity

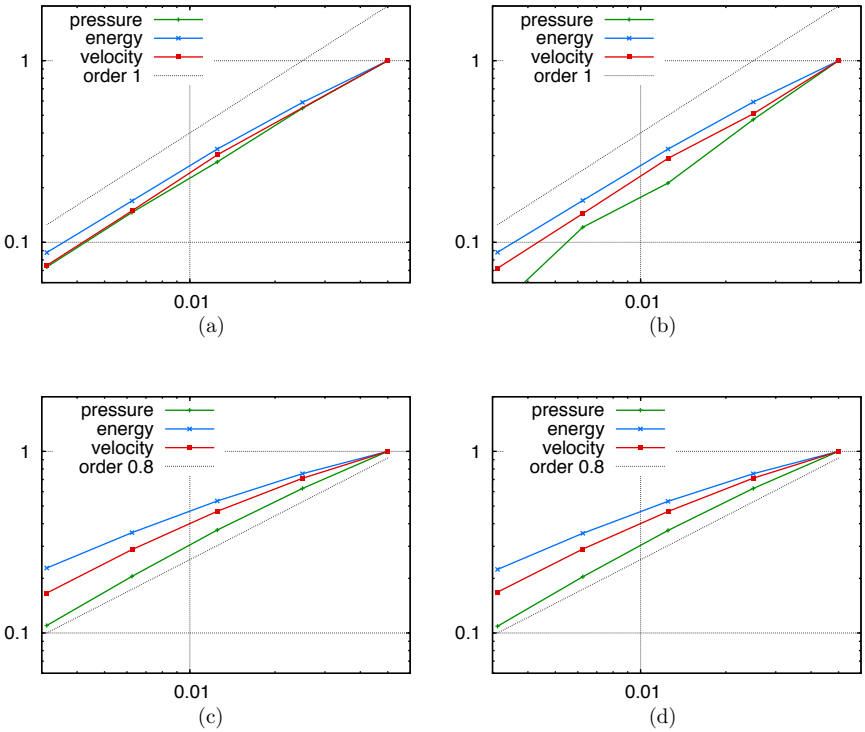

FIGURE 5.1. Numerical errors in the Navier-Stokes (plots (a) and (b)) and Euler cases (plots (c) and (d)), for a Mach number in the range of unity (plots (a) and (c)) or lower than 0.01 (plots (b) and (d)).

is set to $\mu = 0.001$, which roughly corresponds to a fifth of the numerical viscosity introduced by the classical upwinding $\mu_{\text{upw}} \simeq \rho\,|\boldsymbol{u}|\,h/2$ of the convection term.

At first glance, the results are comparable to those presented in the recent literature [7, 16, 49, 6]. As could be expected, the stability of the scheme seems to be paid by a greater diffusion: some authors observe a Kelvin-Helmholtz instability at the contact discontinuity line issued from the Mach triple point (whose occurrence, even in the absence of any shear-stress, is plausible, since the slip line is unstable) which does not appear here, and we also obtain a spurious Mach reflection at the bottom boundary, probably caused by perturbations issued from the step corner. One way to circumvent this problem would be to use (nonconforming) local mesh refinement; the development of such a scheme is underway.

Pressure correction schemes are known to generate spurious boundary conditions for the pressure, which, for the discretization used here, are implicit in the pressure elliptic operator in the correction step (see [10, Section 2.3] for a discussion on this topic, with the same space discretization as here but for the toy problem of the time-dependent incompressible Stokes equations, and Appendix C of the present paper). For a free outlet boundary (as for a Neuman condition), the artificial boundary condition is a non-homogeneous Dirichlet boundary condition for the pressure, with the prescribed value p_{ext} corresponding to the external pressure used in the gradient approximation at the boundary faces. This boundary condition may be observed on Figure 5.2 to generate a very narrow boundary

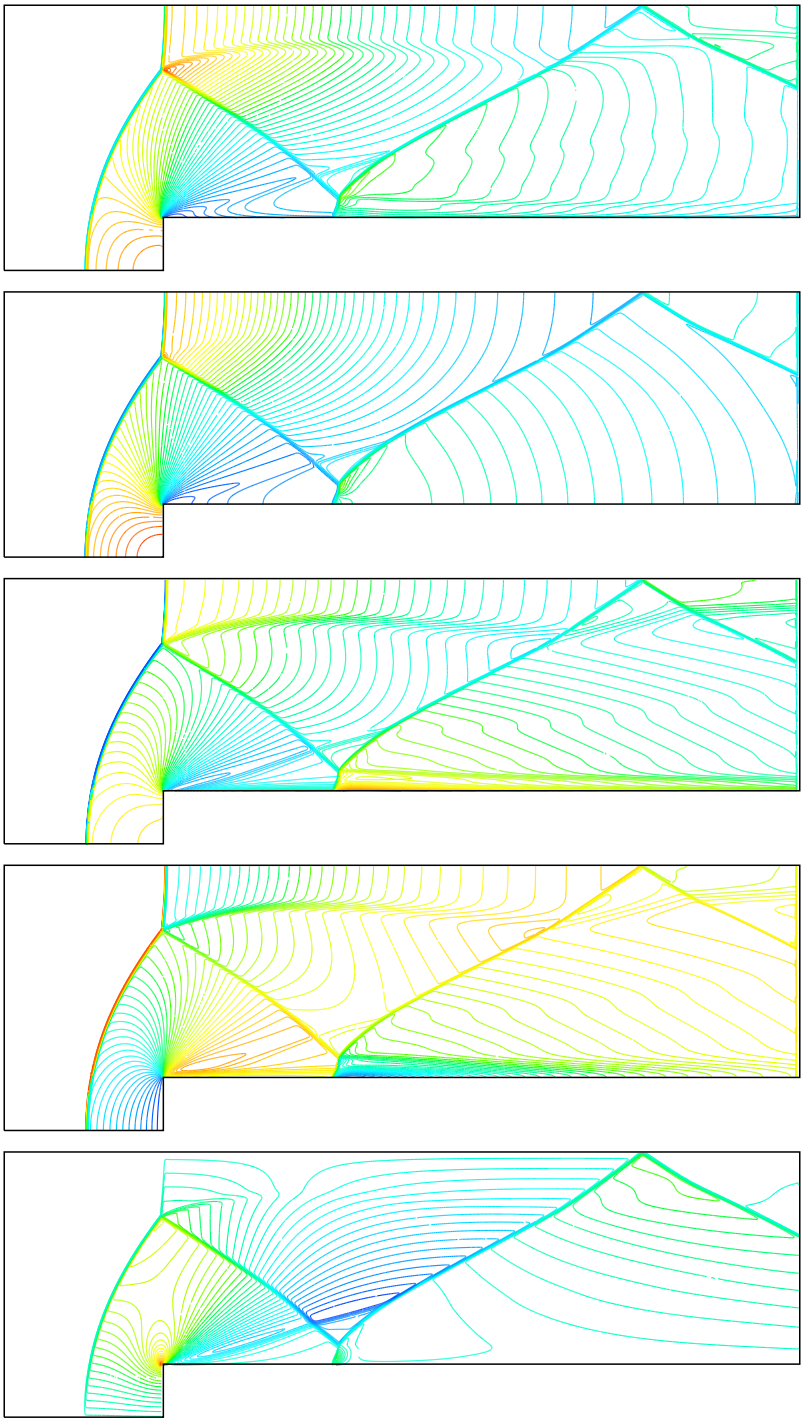

FIGURE 5.2. Mach 3 step – From top to bottom: density, pressure, enthalpy ($\mathcal{H} = e + p/\rho$), first and second component of the velocity at $t = 4$, obtained with $h = 2.5 \times 10^{-3}$, $\delta t = 10^{-3}$ and $\mu = 10^{-3}$. The variation intervals of the unknowns are $\rho \in [0.235,\ 6.4]$, $p \in [0.216,\ 12.04]$, $\mathcal{H} \in [2.46, 8.11]$, $u_1 \in [0.,\ 3.046]$, and $u_2 \in [-0.92,\ 1.82]$.

layer near the outlet section, but without any effect in the remainder of the domain. A similar behaviour was already observed for a similar scheme in the case of barotropic flows [28, Section 4].

5.3. **The double Mach reflection**

We now consider the classical test case (*e.g.* [16]) of a Mach=10 shock in air ($\gamma = 1.4$) impinging a wall with a 60° angle. The right state (pre-shock) initial conditions correspond to a fluid at rest and the left state is given by the Rankine-Hugoniot conditions, supposing that the velocity of the shock is $\omega = 10$ (while the speed of sound in the pre-shock state is $c = 1$, hence the denomination "Mach=10 shock"):

$$\begin{bmatrix} \rho_L \\ \boldsymbol{u}_L \\ p_L \end{bmatrix} = \begin{bmatrix} 8 \\ 8.25\ (\sqrt{3}/2, 1/2)^t \\ 116.5 \end{bmatrix}, \qquad \begin{bmatrix} \rho_R \\ \boldsymbol{u}_R \\ p_R \end{bmatrix} = \begin{bmatrix} 1.4 \\ (0,0)^t \\ 1 \end{bmatrix}.$$

The computational domain is $\Omega = (0,4) \times (0,1)$, as shown in Figure 5.3. The reflecting wall lies

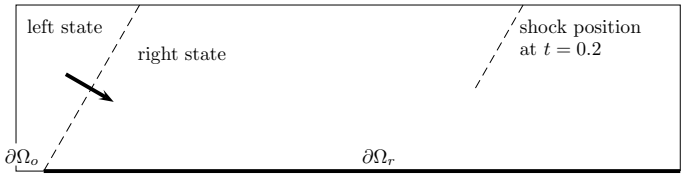

Figure 10. Double Mach reflection – Geometry and initial conditions.

Figure 5.3. Double Mach reflection – Geometry and initial conditions.

at the bottom of the domain and starts at $x_1 = 1/6$, i.e. impermeability and free slip boundary conditions are enforced on $\partial\Omega_r = (1/6, 4) \times \{0\}$ and outflow boundary conditions are prescribed at $\partial\Omega_o = (0, 1/6) \times \{0\}$. At $t = 0$, the shock impinges the reflecting wall (at $x_1 = 1/6$), so the fluid is in the left state for $x_1 \leq 1/6 + x_2/\sqrt{3}$ and in the right state in the rest of the domain. Then, in the zones of Ω which are not perturbed by the reflections, the shock moves with a velocity equal to $\omega\ (\sqrt{3}/2, -1/2)^t$. The external pressure at the outflow boundary $\partial\Omega_o$ is thus prescribed throughout the transient state to $p_L = 116.5$. On the top of the domain $(0,4) \times \{1\}$, the boundary condition is consistent to the undisturbed shock wave, thus the unknowns ρ, $\boldsymbol{u}$ and p are prescribed to the left state values for $x_1 \leq 1/6 + 1/\sqrt{3} + (2 * \omega/\sqrt{3})\ t$ and to the right state values on the other part of the boundary. Finally, on $\{4\} \times (0,1)$, the velocity is prescribed to $\boldsymbol{u}_R = (0,0)^t$.

We plot on Figure 5.4 the results obtained with the MAC scheme, for $t = 0.2$ with a 1600×400 grid (consisting of square cells) and a time step $\delta t = h/100$. The artificial viscosity is $\mu = 0.01$ (to be compared, for instance, with $\rho_L\, |\boldsymbol{u}_L|\, h/2 = 0.0825$). Once again, the results are comparable to those presented in the recent literature (*e.g.* [16]).

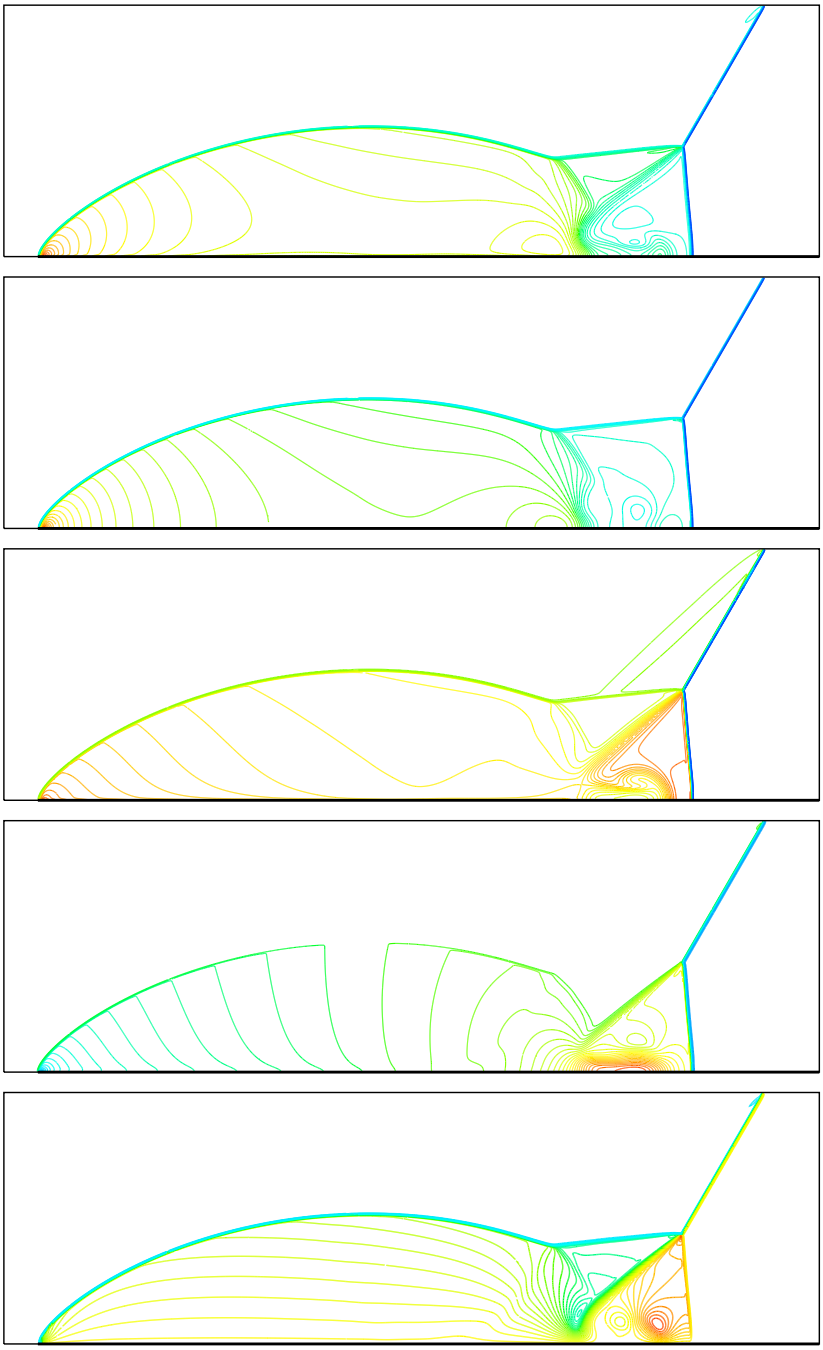

FIGURE 5.4. Double Mach reflection – From top left to bottom right: density, pressure, enthalpy ($\mathcal{H}$) and first and second component of the velocity at $t = 0.2$, obtained with $h = 2.5\ 10^{-3}$, $\delta t = 2.5\ 10^{-5}$ and $\mu = 0.01$. The variation ranges of the unknowns are $\rho \in [1.4,\ 22.4]$, $p \in [1,\ 559]$, $\mathcal{H} \in [2.5,\ 87.8]$, $u_1 \in [-1.74,\ 15.9]$, and $u_2 \in [-5.53,\ 1.74]$. A right part of the domain, where the solution is constant, is not drawn.

5.4. **A two-dimensional Riemann problem**

We address in this section a two-dimensional Riemann problem introduced in [41]. The computational domain is $\Omega = (-0.5, 0.5)^2$ and the initial data consists in four constant states, in each of the four sub-squares of Ω obtained by splitting it along the lines joining the mid-points of each segment of the boundary (*i.e.* in $\Omega_{1,1} = (-0.5, 0) \times (0, 0.5)$, $\Omega_{1,2} = (0, 0.5)^2$, $\Omega_{2,1} = (-0.5, 0)^2$ and $\Omega_{2,2} = (0, 0.5) \times (-0.5, 0)$). These constant states are chosen in such a way that each associated one-dimensional Riemann problem (*i.e.* each one-dimensional problem obtained by picking as left and right initial state the values of ρ, p in two adjacent sub-squares, together with the velocity component normal to the line separating these sub-squares) has for solution a single wave. The four constant states chosen here are:

$\Omega_{1,1}: \ \rho = 1, \ p = 1, \ \boldsymbol{u} = \begin{bmatrix} 0.7276 \\ 0 \end{bmatrix}$	$\Omega_{1,2}: \ \rho = 0.5313, \ p = 0.4, \ \boldsymbol{u} = \begin{bmatrix} 0 \\ 0 \end{bmatrix}$
$\Omega_{2,1}: \ \rho = 0.8, \ p = 1, \ \boldsymbol{u} = \begin{bmatrix} 0 \\ 0 \end{bmatrix}$	$\Omega_{2,2}: \ \rho = 1, \ p = 1, \ \boldsymbol{u} = \begin{bmatrix} 0 \\ 0.7276 \end{bmatrix}$

This configuration is referred to as the configuration 12 in [41]. Two shocks develop, the first one at the interface of $\Omega_{1,1}$ and $\Omega_{1,2}$ and the second one at the interface of $\Omega_{2,2}$ and $\Omega_{1,2}$; they move toward the right and the top of the domain, respectively. The other two interfaces (separating $\Omega_{2,1}$ from $\Omega_{1,2}$ and $\Omega_{2,2}$) do not move with time, and the tangential velocity is different on both sides of the interface; such an interface is called in [41] a slip line, and corresponds to a (steady) contact discontinuity of the system.

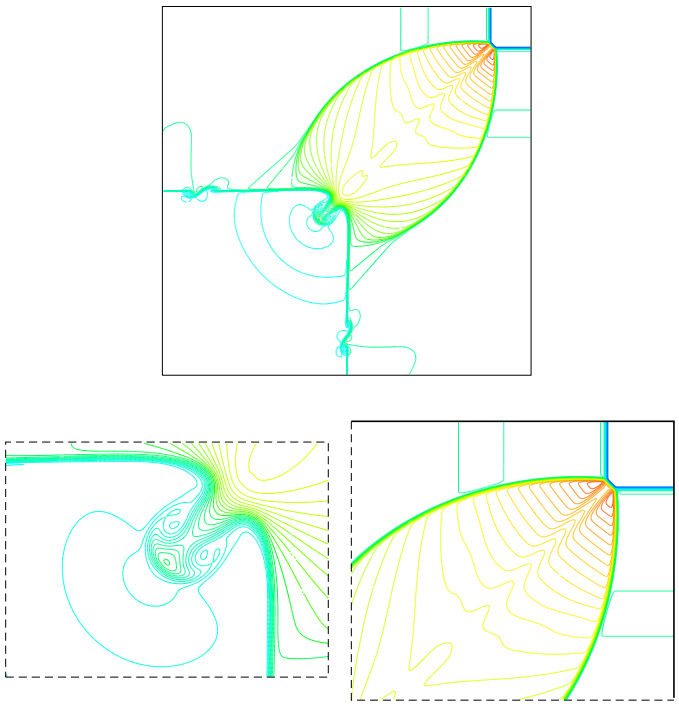

Figure 5.5. 2D Riemann problem – Isolines of the density in the domain, and zoom at the center and the upper right corner of the domain.

Results obtained with the MAC variant of the scheme, a 1000×1000 uniform grid, $\delta t = 2.5\,10^{-4}$ and an artificial viscosity fixed to $\mu = 5\,10^{-5}$ are shown on Figures 5.5 and 5.6. They are in good agreement with reference solutions (*e.g.* [41, 32, 29]). However, the used stabilization technique, namely adding a physical-like artificial diffusion term, generates shear-stress instabilities along the slip lines, as zoomed in Figure 5.6. This seems to be unavoidable, and more elaborate techniques are necessary to avoid this phenomenon. Note however that the solution is not destabilized (in particular, we do not observe the generation of spurious pressure waves polluting the solution in the whole domain). In addition, the problem of computing accurately a standing slip line may look rather academic, since actual difficulties appear when the slip line moves, *i.e.* when the (constant across the line) normal component of the velocity is not zero; up to our knowledge, avoiding significant perturbation of the solution in this latter case indeed remains a challenging issue for numerical Euler solvers (see Appendix B).

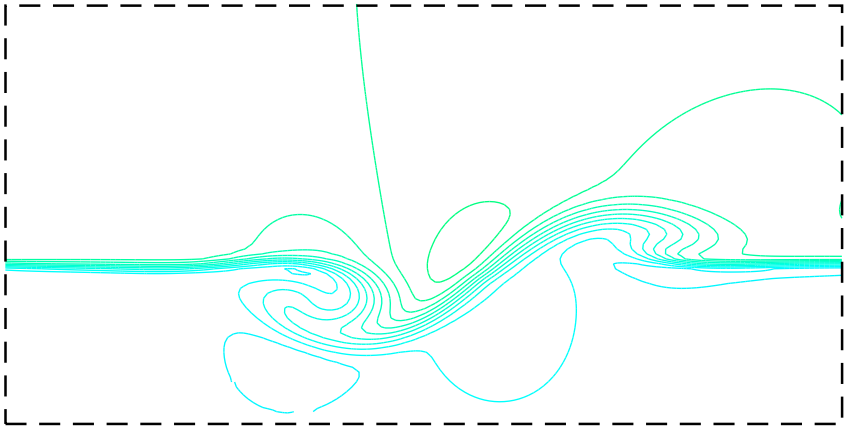

FIGURE 5.6. 2D Riemann problem – Isolines of the density along the horizontal slip line.

5.5. **Navier-Stokes flows past a cylinder**

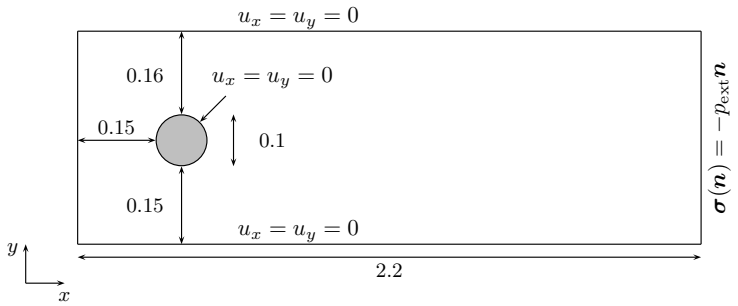

FIGURE 5.7. Low Mach flow past a cylinder – Geometry.

We turn now to the Navier-Stokes equations, and first investigate the accuracy of the scheme in the quasi-incompressible limit. To this purpose, we consider a problem addressed as a benchmark for (incompressible) Navier-Stokes solvers in [40]. The problem is two-dimensionnal, and consists in a flow between two parallel plates past a cylindrical obstacle. The geometry of the problem is described in Figure 5.7. The fluid enters the domain on the left boundary, with an imposed velocity profile:

$$\boldsymbol{u} = (4u_m y \frac{H-y}{H^2}, 0)^t,$$

where $H = 0.41$ is the height of the channel and $u_m = 1.5$; the velocity is prescribed to zero at the other boundaries except for the right-hand side, where we use a Neuman boundary condition:

$$(\boldsymbol{\tau}(\boldsymbol{u}) - p\,\boldsymbol{I})\ \boldsymbol{n} = -p_{\text{ext}}\,\boldsymbol{n},$$

where p_{ext} stands for a given external pressure. The initial pressure and p_{ext} are set both to 10^5, and the initial density is $\rho = 1$. With these values, the sound speed $c = (\gamma p/\rho)^{1/2}$ is $c \simeq 370$, so the characteristic Mach number is close to 0.003. The viscosity is $\mu = 0.001$, so the Reynolds number, defined as $Re = \rho \bar{u} D/\mu$, where $D = 0.1$ is the diameter of the cylinder and $\bar{u} = 2u_x(0, H/2)/3$, is equal to 100.

A "coarse version" of the meshes used for the presented computation is sketched in Figure 5.8; real meshes are considerably refined with respect to this one, by diminishing the discretization step along the characteristic lines (the boundaries and the concentric circles around the cylinder). In all the computations, we set the time step to $\delta t = 5 \cdot 10^{-4} s$.

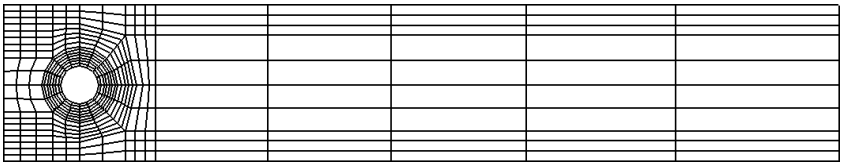

Figure 5.8. A "coarse version" of the mesh.

We observe in our computations the usual vortex-shedding phenomenon, well-known for incompressible flows (the so-called Von-Karmann alley), and the pressure and density show very small variations in space (the difference between the maximum and minimum value for the pressure and the density in the domain is in the range of 2 and 3.10^{-5} respectively). To assess in a quantitative way the accuracy of the results, we compute some characteristic flow quantities. The drag and lift coefficients, denoted by c_d and c_l respectively, are given by

$$c_d = \frac{2F_d}{\rho \bar{u}^2 D}, \qquad c_l = \frac{2F_l}{\rho \bar{u}^2 D},$$

where F_d and F_l are the drag and lift forces respectively:

$$F_d = \int_{\mathcal{D}} (\mu \frac{\partial u_t}{\partial n} n_y - p n_x)\, \mathrm{d}\gamma, , \qquad F_l = \int_{\mathcal{D}} (-\mu \frac{\partial u_t}{\partial n} n_x - p n_y)\, \mathrm{d}\gamma.$$

with $\mathcal{D}$ the disk surface, $\boldsymbol{n} = (n_x, n_y)^t$ its outward normal vector and u_t the velocity in the direction tangent to the disk, *i.e.* collinear to $\boldsymbol{t} = (n_y, -n_x)^t$. In Table 5.1 below, we denote by $c_{d,max}$ and $c_{l,max}$ the maximum absolute values of these coefficients. The Strouhal number is defined as $St = Df/\bar{u}$, where f is the frequency of separation, calculated directly from the period of F_l. We gather in Table 5.1 the obtained values for these parameters for different meshes, together with their plausible range derived from the set of the contributions to the benchmark [40]. Values entering this reference interval

are typeset in bold. The present algorithm seems as accurate as the incompressible pressure-correction solver based on the same space discretization studied in [2].

Mesh	Space unks	$c_{d,max}$	$c_{l,max}$	St
m2	64840	3.4937	0.9141	0.2850
m3	215545	3.2887	0.9891	**0.2955**
m4	381119	3.2614	**1.0062**	**0.2972**
m5	531301	**3.2365**	**1.0148**	**0.2976**
Reference range		3.22 - 3.24	0.99 - 1.01	0.295 - 0.305

Table 5.1. Characteristic flow quantities.

We now turn to a compressible version of this test, with a high characteristic Mach number, close to Ma= $\sqrt{10}$. To this purpose, we set the initial pressure and the external pressure p_{ext} at the value $\gamma/10\,\rho$, so that the sound speed is now given by $c^2 = 0.1$. In this case, since the heating on the surface of the cylinder is important, we prescribe the internal energy at its inlet value at the surface of the disk, and fix the thermal conductivity of the fluid to $\lambda = 10^{-3}$. To avoid to complicate the flow structure near the domain boundaries, we impose an impermeability and perfect slip condition at the upper and lower boundaries and the inlet velocity is prescribed to a constant in space (and time) value $\boldsymbol{u} = (1, 0)^t$. The time step is $\delta t = 10^{-4}$. The rest of the configuration is unchanged, and the initial values are still the same as the inlet values.

Results obtained at $t = 5$ with a mesh of about 10^6 cells are shown on Figures 5.9 and 5.10. We observe a strong shock upstream the disk, with a Mach reflection at the upper and lower boundaries. Subsequent (downstream) reflections yield "*X-structures*" for the pressure field; they are progressively damped, both by the physical viscosity and (probably) by the scheme diffusion. As in the Euler case, the artificial boundary conditions imposed by the pressure correction technique to the pressure at the outlet section spoil the flow only on a narrow (numerical) boundary layer.

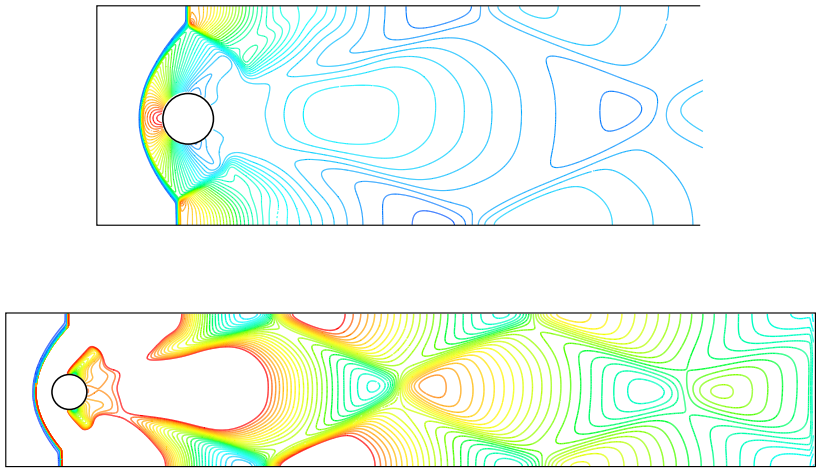

FIGURE 5.9. Mach=10 flow past a cylinder – Top: iso-lines of pressure near the disk ($p \in (0.0713,\ 0.957)$) at $t = 5$; bottom: still pressure iso-lines but on the whole computational domain, and restricted to the interval $(0.0713,\ 0.2)$) (so the areas left in white on the figure correspond to zones where $p > 0.2$).

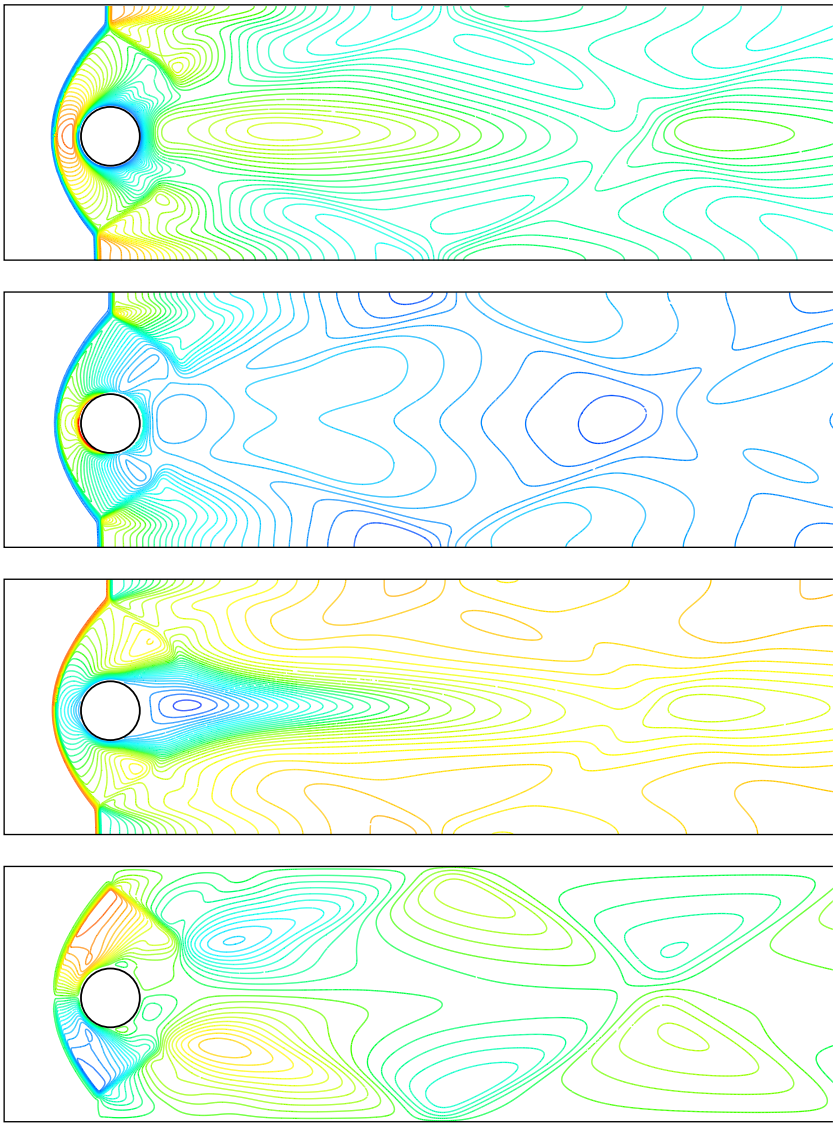

FIGURE 5.10. Mach=10 flow past a cylinder – From top to bottom: internal energy, density, x-component of velocity, y-component of velocity at $t = 5$. The variation ranges of the unknowns are $e \in [0.178,\ 0.536]$, $\rho \in [0.804,\ 12.23]$, $u_1 \in [-0.11,\ 1]$, and the value $u_1 = 0$ corresponds to the fourth iso-line starting from the center of the vortex attached to the cylinder, $u_2 \in [-0.326,\ 0.327]$.

5.6. **Interaction of a shock and a cube**

To conclude this section, we turn to a three-dimensional problem, which consists in the interaction of a shock wave and a cube. We consider the same pure shock wave as for the double Mach reflection problem, which now travels in the x_1-direction:

$$\begin{bmatrix} \rho_L \\ \boldsymbol{u}_L \\ p_L \end{bmatrix} = \begin{bmatrix} 8 \\ 8.25\ (1,0,0)^t \\ 116.5 \end{bmatrix}, \qquad \begin{bmatrix} \rho_R \\ \boldsymbol{u}_R \\ p_R \end{bmatrix} = \begin{bmatrix} 1.4 \\ (0,0,0)^t \\ 1 \end{bmatrix},$$

and $(\rho, \boldsymbol{u}, p) = (\rho_L, \boldsymbol{u}_L, p_L)$ (resp. $(\rho, \boldsymbol{u}, p) = (\rho_R, \boldsymbol{u}_R, p_R)$) for $x_1 \leq -1.3$ (resp. $x_1 \geq -1.3$). The obstacle is the cube $(-1,1)^3$. Since the problem presents two symmetry planes, defined by $x_2 = 0$ and $x_3 = 0$ respectively, the chosen computational domain is $\Omega = (-3,5) \times (0,4) \times (0,4)$. The cells are cubes of edges 0.02 long, which leads to a $400 \times 200 \times 200$ uniform grid from which the cells corresponding to the interior of the obstacle have been removed; the mesh finally includes 15 750 000 control volumes. The final time is $T = 0.6$ (remember that, in absence of obstacle, the shock speed is equal to 10, so the front location at the final time should be the plane $x_1 = 4.7$), and the chosen time step is $\delta t = 0.0005$, which corresponds to a CFL number close to 1/3 with respect to the maximum wave celerity in the left state ($c \simeq 4.5$). The MAC scheme is used for the space discretization, and the convection operator in the momentum balance equation is centered and stabilized with an artificial viscosity $\mu = 0.5$ (lower than the diffusion entailed by the classical upwinding $\rho\,|\boldsymbol{u}|\,h/2$ of this term, which is greater than 1 locally in space and time during the computation).

The obtained pressure field is shown on Figures 5.11 and 5.12. A strong reflection is observed on the obstacle: the maximum pressure rises to $p \simeq 900$ at the first reflections, and then progressively decreases to $p \simeq 500$. Then the pressure wave overpasses the obstacle, and a "shock-against-shock" recomposition is observed at a time close to $t = 0.45$ (first illustration on Figure 5.11) at the intersection of the symmetry planes, which leads to a maximum pressure close to the pressure observed on the left face of the obstacle, *i.e.* $p \simeq 500$; the pressure field at $t = 0.456$ on the plane $x_1 = 2$ (so at a distance of 1 after the obstacle) is shown on Figure 5.12. This recomposition leads to an irregular Mach reflection, which clearly appears later (second illustration on Figure 5.11, $t = 0.6$).

Since this test is representative of industrial applications, we now give some information about the numerical resolution. The computation is performed in parallel (the CALIF^{3}S software uses PETSc primitives) on an infiniband linux cluster and involves 60 Intel Xeon X5660 2.8GHz processors, for about 14 hours of restitution time. The solution of the linear system for the prediction step is performed with a GMRES algorithm, preconditioned on each subdomain by ILU0; the solution of the system takes about 1.5 hours (cumulated over the 1200 time steps), for about $47\,10^6$ unknowns (the degrees of freedom of the 3 components of the velocity, which are coupled in the same system, to allow the discretization of the viscous tensor under its general form, used here only for stabilization purposes). The correction step is solved by a Newton algorithm (see Appendix C), which converges in 4 to 5 iterations. Each internal system is solved by the same GMRES solver as in the prediction step, with now about $30\,10^6$ unknowns (pressure and internal energy degrees of freedom), for a cumulated time close to 3.3 hours. The rest of the CPU time (about 8 hours) is used for the assembling of these systems.

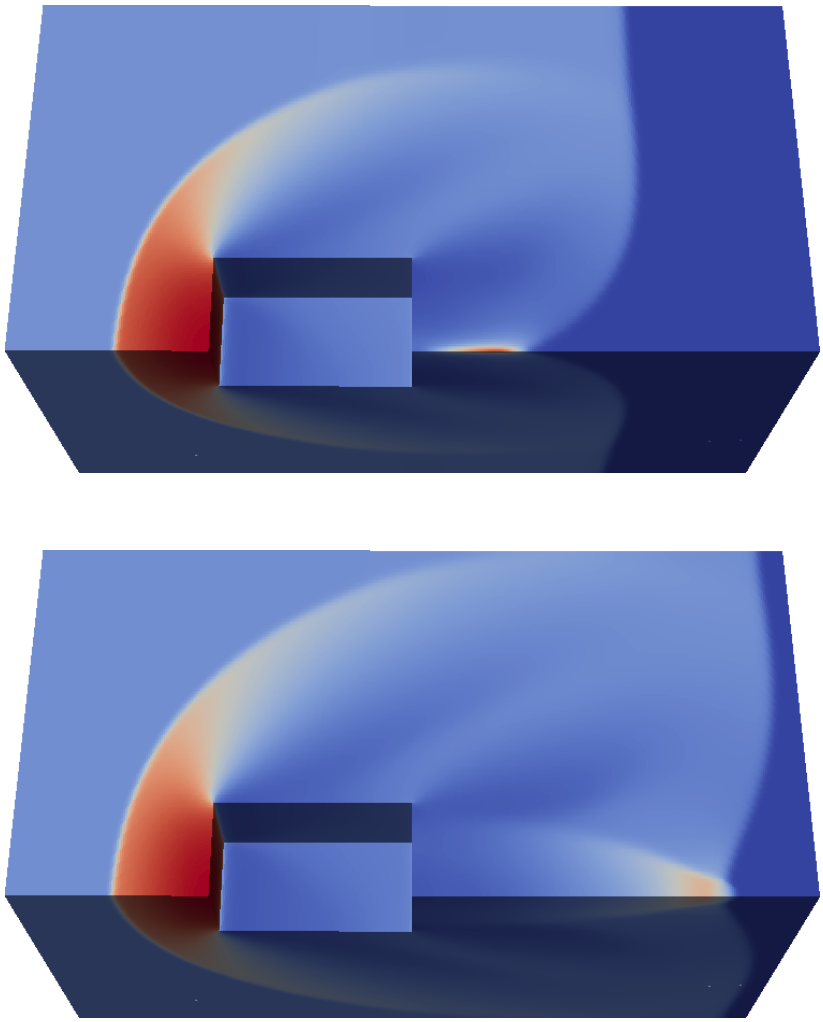

FIGURE 5.11. Interaction between a shock and a cube – Pressure on the symmetry planes $x_=20$ and $x_3 = 0$ at times $t = 0.456$ (top) and $t = 0.6$ (bottom).

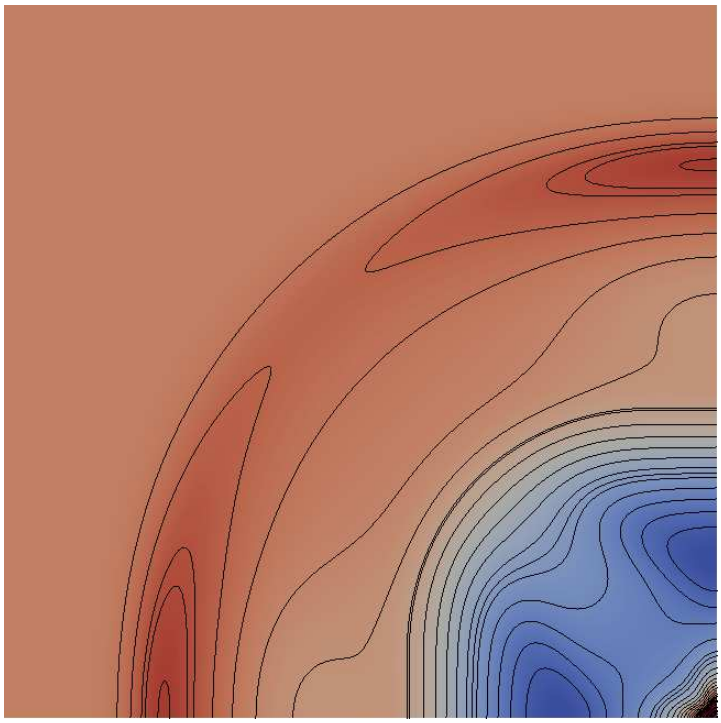

Figure 5.12. Interaction between a shock and a cube – Pressure at $t = 0.456$ on the plane $x_1 = 2$.

Appendix A. Pressure correction methods and kinetic energy balance

When applying a pressure correction method to the computation of a variable density flow, a specific treatment of the pressure is necessary to obtain a kinetic energy identity. To this purpose, an *ad hoc* technique was introduced in [15] and, to our knowledge, it is still today the only work on this topic. We propose here a different method, and briefly compare it with the algorithm described in [15].

To present the difficulty which we face, let us work in the time semi-discrete formalism, and let us denote by $\overline{\boldsymbol{\nabla}} p^{n+1}$ the pressure gradient used in the velocity prediction step, postponing its definition for a while. Let us also denote by $\mathcal{C}(\tilde{\boldsymbol{u}}^{n+1})$ the convection operator for the velocity, and let us suppose that this operator satisfies an identity of the form:

$$\mathcal{C}(\tilde{\boldsymbol{u}}^{n+1})\cdot\tilde{\boldsymbol{u}}^{n+1}=\frac{1}{2\,\delta t}\Big[\rho^{m+1}|\tilde{\boldsymbol{u}}^{n+1}|^2-\rho^m|\boldsymbol{u}^n|^2\Big]+\frac{1}{2}\mathrm{div}(|\tilde{\boldsymbol{u}}^{n+1}|^2\,\boldsymbol{q}^\ell)+\mathcal{R}^{n+1},\tag{A.1}$$

where ℓ and m stand for time indices depending on n and $\boldsymbol{q}^\ell$ stands for an approximation of the mass flux, and with $\mathcal{R}^{n+1}\geq 0$. In the present paper, we have:

$$\mathcal{C}(\tilde{\boldsymbol{u}}^{n+1})=\frac{1}{\delta t}(\rho^n\tilde{\boldsymbol{u}}^{n+1}-\rho^{n-1}\boldsymbol{u}^n)+\mathrm{div}(\rho^n\tilde{\boldsymbol{u}}^{n+1}\otimes\boldsymbol{u}^n),$$

and Relation (A.1) is satisfied with $m=n-1$ and $\boldsymbol{q}=\rho\,\boldsymbol{u}$, $\ell=n$. Other choices for the convection operator are possible [15, 33, 35]. With the above notations, the velocity prediction step reads:

$$\mathcal{C}(\tilde{\boldsymbol{u}}^{n+1})-\mathrm{div}(\boldsymbol{\tau}(\tilde{\boldsymbol{u}}^{n+1}))+\overline{\boldsymbol{\nabla}} p^{n+1}=0.\tag{A.2}$$

Our aim here is to obtain a discrete equivalent of the kinetic energy balance, which we recall:

$$\frac{1}{2}\partial_t(\rho\,|\boldsymbol{u}|^2)+\frac{1}{2}\mathrm{div}(\rho\,|\boldsymbol{u}|^2\,\boldsymbol{u})-\mathrm{div}(\boldsymbol{\tau}(\boldsymbol{u}))\cdot\boldsymbol{u}+\boldsymbol{\nabla} p\cdot\boldsymbol{u}=0.\tag{A.3}$$

This relation is obtained by taking the inner product of the momentum balance equation by the velocity. Thus, let us take the inner product of (A.2) by $\tilde{\boldsymbol{u}}^{n+1}$. Using (A.1), we get:

$$\begin{aligned}\frac{1}{2\,\delta t}\Big[\rho^{m+1}|\tilde{\boldsymbol{u}}^{n+1}|^2-\rho^m|\boldsymbol{u}^n|^2\Big]+\frac{1}{2}\mathrm{div}(|\tilde{\boldsymbol{u}}^{n+1}|^2\,\boldsymbol{q}^\ell)&\\ -\mathrm{div}(\boldsymbol{\tau}(\tilde{\boldsymbol{u}}^{n+1}))\cdot\tilde{\boldsymbol{u}}^{n+1}+\overline{\boldsymbol{\nabla}} p^{n+1}\cdot\tilde{\boldsymbol{u}}^{n+1}&=-\mathcal{R}^{n+1}.\end{aligned}\tag{A.4}$$

This relation is not a discrete analogue of (A.3), since the first two terms cannot be interpreted as a discrete time derivative, due to the presence in the first term of $|\tilde{\boldsymbol{u}}^{n+1}|^2$ instead of $|\boldsymbol{u}^{n+1}|^2$. Hence, we now turn to the correction step, and write the velocity correction equation as:

$$\frac{1}{\delta t}\,\rho^{m+1}\boldsymbol{u}^{n+1}+\boldsymbol{\nabla} p^{n+1}=\frac{1}{\delta t}\,\rho^{m+1}\tilde{\boldsymbol{u}}^{n+1}+\overline{\boldsymbol{\nabla}} p^{n+1}.$$

Let us multiply this relation by $[\delta t/(2\rho^{m+1})]^{1/2}$ and square the resulting equation, to obtain:

$$\begin{aligned}\frac{1}{2\delta t}\,\rho^{m+1}|\boldsymbol{u}^{n+1}|^2+\boldsymbol{\nabla} p^{n+1}\cdot\boldsymbol{u}^{n+1}+\frac{\delta t}{2\rho^{m+1}}\,|\boldsymbol{\nabla} p^{n+1}|^2&\\ =\frac{1}{2\delta t}\,\rho^{m+1}|\tilde{\boldsymbol{u}}^{n+1}|^2+\overline{\boldsymbol{\nabla}} p^{n+1}\cdot\tilde{\boldsymbol{u}}^{n+1}+\frac{\delta t}{2\rho^{m+1}}\,|\overline{\boldsymbol{\nabla}} p^{n+1}|^2.&\end{aligned}$$

Adding this relation with (A.4), we get:

$$\begin{aligned}\frac{1}{2\,\delta t}\Big[\rho^{m+1}|\boldsymbol{u}^{n+1}|^2-\rho^m|\boldsymbol{u}^n|^2\Big]+\frac{1}{2}\mathrm{div}(|\tilde{\boldsymbol{u}}^{n+1}|^2\,\boldsymbol{q}^\ell)&\\ -\mathrm{div}(\boldsymbol{\tau}(\tilde{\boldsymbol{u}}^{n+1}))\cdot\tilde{\boldsymbol{u}}^{n+1}+\boldsymbol{\nabla} p^{n+1}\cdot\boldsymbol{u}^{n+1}&=-\mathcal{R}^{n+1}-\mathcal{R}_{\boldsymbol{\nabla}}^{n+1}.\end{aligned}\tag{A.5}$$

with:

$$\mathcal{R}_{\boldsymbol{\nabla}}^{n+1} = \frac{\delta t}{2\rho^{m+1}} |\boldsymbol{\nabla} p^{n+1}|^2 - \frac{\delta t}{2\rho^{m+1}} |\overline{\boldsymbol{\nabla}} p^{n+1}|^2.$$

Equation (A.5) is now a discrete analogue to (A.3). However, it is interesting to recast $\mathcal{R}_{\boldsymbol{\nabla}}^{n+1}$ as a difference of the same quantity at two different time levels, for at least two reasons:

- first, summing (A.5) in time, we obtain in this case a stability estimate.
- Second, if Relation (A.5) is multiplied by a regular test function, lest us say φ^{n+1}, and, once again, summed in time, a discrete integration by parts in time makes δt times the (discrete) time derivative of φ appear. The factor δt is decisive to prove that the corresponding sum, *i.e.* the sum over n of $\mathcal{R}_{\boldsymbol{\nabla}}^{n+1}\ \varphi^{n+1}$, tends to zero, even for an irregular (shock) solution. No counterpart of the remainder term $\mathcal{R}_{\boldsymbol{\nabla}}^{n+1}$ thus needs to be introduced in the internal energy balance in the case of the Euler equations.

To reach this goal, we thus need to have:

$$\frac{\delta t}{2\rho^{m+1}} |\overline{\boldsymbol{\nabla}} p^{n+1}|^2 = \frac{\delta t}{2\rho^{m}} |\boldsymbol{\nabla} p^{n}|^2$$

which yields the following definition for $\overline{\boldsymbol{\nabla}} p^{n+1}$:

$$\overline{\boldsymbol{\nabla}} p^{n+1} = \Big[\frac{\rho^{m+1}}{\rho^m}\Big]^{1/2}\ \boldsymbol{\nabla} p^n. \tag{A.6}$$

Note that this quantity is not necessarily the (discrete) gradient of a discrete pressure field (hence, the notation $\overline{\boldsymbol{\nabla}} p$ instead of $\boldsymbol{\nabla} \overline{p}$).

Finally, we thus only need to multiply the beginning-of-step pressure gradient by a factor (hopefully known, which is the case here with $m = n - 1$), which almost leaves unchanged the count of algebraic operations associated to a time step.

On the contrary, the method proposed in [15] consists in solving for $\overline{p}^{n+1}$ the following elliptic problem:

$$\mathrm{div}\Big[\frac{1}{\rho^{m+1}} \boldsymbol{\nabla} \overline{p}^{n+1}\Big] = \mathrm{div}\Big[\frac{1}{(\rho^{m+1}\,\rho^m)^{1/2}} \boldsymbol{\nabla} p^n\Big]. \tag{A.7}$$

By more intricate arguments than for (A.6) (especially for the issue of the introduction of corrective terms in the internal balance energy), it may be shown that (A.7) provides the same benefits as (A.6) [27]. In addition, in one space dimension, both relations yields the same corrected gradient (*i.e.* $\overline{\boldsymbol{\nabla}} p^{n+1} = \boldsymbol{\nabla} \overline{p}^{n+1}$).

Remark A.1 (On the choice of m.)**.** In [15], from which Equation (A.7) is extracted, the authors design a scheme for incompressible density varying flows modelled by the incompressible Navier-Stokes equations complemented by a transport equation for the density. In this case, a natural algorithm is

- first update ρ by solving the associated transport equation, with the beginning-of-step velocity,
- then solve Navier-Stokes equations by a projection scheme.

In this case, the choice $m = n$ is natural (and, indeed, $m = n$ in (A.7)). This algorithm has been implemented for the same problem at IRSN, and seems to work quite well.

In past studies, we also designed a more complicated scheme for quasi-incompressible flows, which consists in performing a prediction for the density by solving the mass balance a first time, let say for $\rho^{n+1/2}$, and then use this density in the velocity prediction step (so that $m = n - 1/2$), and finally correct the velocity with once again the mass balance, but with the end-of-step density. This scheme seemed to yield good results, but if it was not conservative for the momentum. More generally, this kind of procedure is often used to get more accuracy with respect to the time discretization (even if

the beneficial effects are not so clear, and the consistency in the hyperbolic limit may become difficult to obtain...).

These examples show that other choices than $m = n - 1$ are possible, and some are found in the literature in the discrete momentum balance equation.

Appendix B. Behaviour of the scheme on contact discontinuities

In this section, we check the ability of the proposed scheme to deal with contact discontinuities without generating numerical perturbations. We forget boundary conditions, or, in other words, suppose that $\Omega = \mathbb{R}^d$, $1 \leq d \leq 3$.

In 1D, this just amounts to check that the scheme is able to propagate a discontinuity for ρ and e while keeping the velocity and the pressure constant. Let us thus suppose that, at the time level n, u^n and p^n are constant, let us say $u^n \equiv \bar{u}$ and $p^n \equiv \bar{p}$, and let us examine the consequences of this assumption in the scheme (3.1):

- Since the pressure gradient $\boldsymbol{\nabla} p^n$ vanishes, so does $\overline{\boldsymbol{\nabla}} p^{n+1}$;
- Thanks to the fact that the convection operator in the momentum balance equation (3.1b) vanishes for constant advected fields $\tilde{u}^{n+1}$ (or, in other words, thanks to the fact that the mass balance over dual cells (3.5) holds), we obtain that $\tilde{u}^{n+1} \equiv \bar{u}$. In addition, the expression (4.2) of the remainder terms (R_σ^{n+1}) shows that they vanish, and so do the corrective terms (S_K^{n+1}) (see Equation (4.3)).
- Let us now suppose that the equation of state is such that the product ρe is a function of the pressure only:
$$\rho e = f(p). \tag{B.1}$$
Typical exampled of such a situation are perfect gases ($p = (\gamma - 1)\rho e$) or stiffen gases ($p = (\gamma - 1)\rho e + \gamma p_\infty$, with p_∞ a fixed positive constant). Then it is easy to see the $p^{n+1} \equiv \bar{p}$ and $u^{n+1} \equiv \bar{u}$ satisfy Equations (3.1c) and (3.1e). Equation (3.1d) can then be seen as a transport equation (since u^{n+1} is constant) and yields ρ^{n+1} while the equation of state yields e^{n+1}.

This shows that the pressure and velocity remain constant through contact discontinuities, provided that the assumption (B.1) holds.

Let us now turn to the two-dimensional case. The preceding reasoning still holds for the specific solutions where $\boldsymbol{u}$ and p are constant and ρ and e are transported. We now consider the contact discontinuity wave (specific to the two-dimensional case) which consists of the transport of one component of the velocity, let us say $\boldsymbol{u} \cdot \boldsymbol{t}$, by a velocity field constant in the direction $\boldsymbol{n}$, with $\boldsymbol{n} \cdot \boldsymbol{t} = 0$. For instance, such a situation is obtained for the initial data:

$$\rho_0 = 1,\ p_0 = 1,\ \boldsymbol{u} = \begin{bmatrix} 1 \\ 5 \end{bmatrix} \text{ on } (-\infty, 0) \times \mathbb{R} \text{ and } \boldsymbol{u} = \begin{bmatrix} 1 \\ -5 \end{bmatrix} \text{ on } (0, +\infty) \times \mathbb{R}.$$

By similar arguments as previously, we would obtain that $u_1 \equiv 1$, $\rho \equiv 1$ and $p \equiv 1$ while u_2 is a solution of a transport equation given by the second component of the momentum balance, provided that the corrective terms (S_K^n) identically vanish. Unfortunately, the discrete kinetic energy balance is not exactly satisfied (see the expression (4.2) of the remainder terms), the terms (S_K^n) are not equal to zero, and we cannot expect the constant solution for ρ, p (and e) and u_1 to be preserved. This may be observed on Figure B.1, where we plot the solution obtained with $\Omega = (-0.5, 0.5) \times (-0.5, 0.5)$, a mesh consisting of 3 horizontal stripes of $n = 500$, $n = 1000$ and $n = 2000$ cells, at $t = 0.12$. The equation of state is:

$$p = (\gamma - 1)\rho e, \quad \gamma = 1.4,$$

so that the constant sound speed satisfies $c^2 = 1.4$. The time step is set to $\delta t = 1/(4n)$ (the CFL number is therefore close to 1/2), and the artificial viscosity is set to $\mu = 1/(40n)$ (so 20 times lower than the viscosity which would be generated by an upwind discretization of the velocity convection term). As shown by the profile for u_2, this diffusion is sufficient to damp most of the oscillations which should be generated by the transport of a discontinuity by a centered convection operator. Numerically, we observe a strong heating at the contact discontinuity, which leads to a strong decrease of the density, and subsequent perturbations on the pressure and the horizontal velocity (recall that these quantities are constant in the continuous solution). The difference between the numerical and the exact solutions seems to be only bounded in the L^∞-norm (in fact, for ρ and e only) and to tend to zero in L^1 (and therefore in L^p, for any finite p).

To the best of our knowledge, the observed behaviour is common to all Euler solvers. Moreover, the previous analysis shows that, to avoid perturbations, the scheme should satisfy an exact discrete kinetic balance (*i.e.* without remainder term). As soon as ρ is constant, this can be achieved by switching from a backward Euler to a Crank-Nicolson time discretization of the momentum balance and setting to zero the artificial viscosity [2]; however, it is of little interest, since the second component of the velocity then suffers from numerical oscillations and, essentially, since ρ varies across a contact discontinuity in the general case. For our scheme, a solution could be also to arbitrarily set the corrective terms (S_K^n) to zero, since they are probably not necessary *at contact discontinuities* to the consistency of the scheme (indeed, contrary to what happens at shocks, they are expected to tend to zero in L^1 as the mesh and time steps tend to 0, see Remark 4.2); however, this would require to be able to distinguish dynamically (*i.e.* in view of the results, during the computation) a contact discontinuity from a shock, which does not seems to be an easy task.

Appendix C. Numerical solution of the correction step

Case of the Euler equations, $\rho e = f(p)$ – When the equation of state is such that the product ρe is a function of the pressure only, and in the absence of heat diffusion (*i.e.* $\lambda = 0$), the correction step may be solved in two decoupled substeps:

- **First step** - From Equation (3.1c), the end-of-step velocity may be written as a function of the end-of-step pressure (and of known quantities). Inserting this expression in the internal energy balance (3.1e) yields a discrete nonlinear parabolic problem for the pressure only, which thus allows to compute p^{n+1}. Then, (3.1c) gives $\boldsymbol{u}^{n+1}$.
- **Second step** - The mass balance (3.1d) is now a linear problem for ρ^{n+1} (or $1/e^{n+1}$), and the equation of state finally yields e^{n+1} (or ρ^{n+1}).

Let us now write the discrete parabolic problem for the pressure as:

$$\forall K \in \mathcal{M}, \quad \frac{|K|}{\delta t}\left[f(p_K^{n+1}) - f(p_K^n)\right] + \sum_{\sigma \in \mathcal{E}(K)} G_{K,\sigma}^{n+1} = S_K^{n+1}. \tag{C.1}$$

Let us now give the expression of each term of this equation. From (3.1c), we get:

$$\text{For } 1 \le i \le d,\ \forall \sigma \in \mathcal{E}_{\mathcal{S}}^{(i)}, \qquad u_{\sigma,i}^{n+1} = \tilde{u}_{\sigma,i}^{n+1} - \frac{\delta t}{\rho_{D_\sigma}^n}\,\boldsymbol{\nabla}_{\sigma,i}(p^{n+1}) + \frac{\delta t}{\rho_{D_\sigma}^n}\,\overline{\boldsymbol{\nabla}}_{\sigma,i}(p^{n+1}).$$

Considering only the normal component of the velocity at the face and using the definition (3.6) of the discrete gradient, we get:

$$\forall \sigma = K|L \in \mathcal{E}_{\text{int}}, \quad u_{K,\sigma}^{n+1} = \tilde{u}_{K,\sigma}^{n+1} + \frac{\delta t\ |\sigma|}{\rho_{D_\sigma}^n\ |D_\sigma|}(p_K^{n+1} - p_L^{n+1}) - \frac{\delta t\ |\sigma|}{(\rho_{D_\sigma}^n)^{1/2}(\rho_{D_\sigma}^{n-1})^{1/2}\ |D_\sigma|}(p_K^n - p_L^n),$$

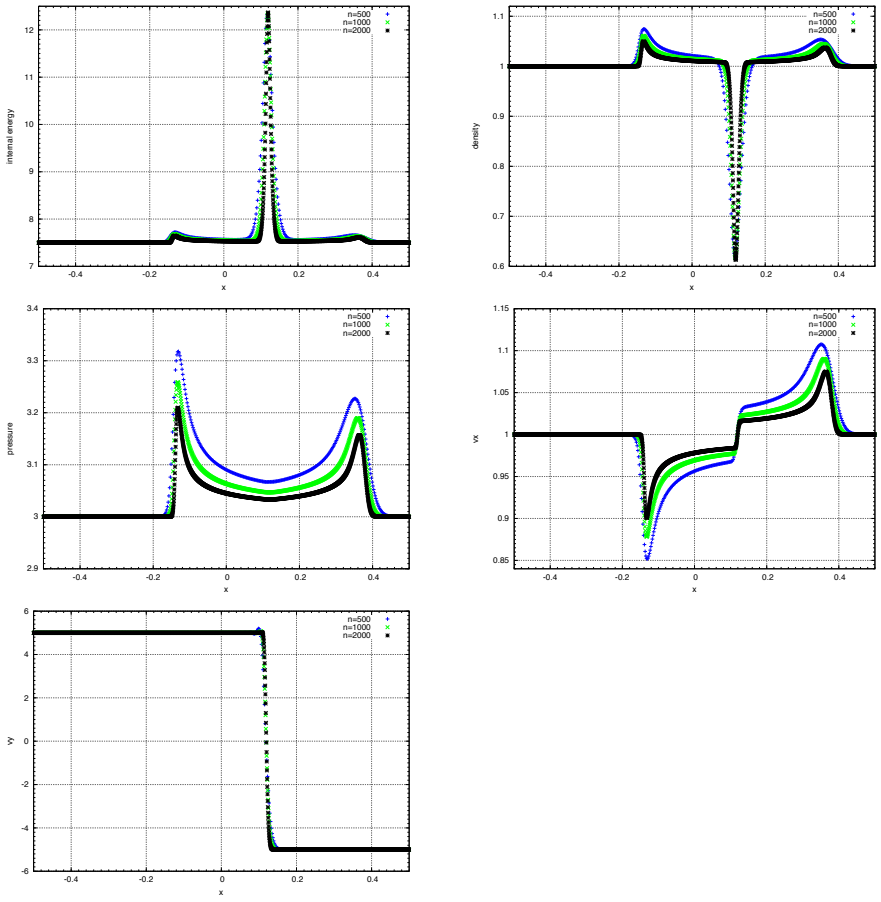

FIGURE B.1. Slip contact discontinuity – Results for $h = 1/500$, $h = 1/1000$ and $h = 1/2000$, along a line parallel to the x-axis. Internal energy (top-left), density (top-right), pressure (middle-left), x-velocity (middle-right) and y-velocity (bottom).

where $\tilde{u}_{K,\sigma}^{n+1}$ is defined according to Relation (3.3). When the normal velocity is prescribed to zero at the external faces, so is the pressure gradient, and thus $u_{K,\sigma}^{n+1} = 0$. Let us denote by $\tilde{v}_{K,\sigma}^{n+1}$ the known part of the right-hand side in the previous relation, *i.e.* :

$$\forall \sigma = K|L \in \mathcal{E}_{\rm int}, \quad \tilde{v}_{K,\sigma}^{n+1} = \tilde{u}_{K,\sigma}^{n+1} - \frac{\delta t\ |\sigma|}{(\rho_{D_\sigma}^n)^{1/2}(\rho_{D_\sigma}^{n-1})^{1/2}\ |D_\sigma|}(p_K^n - p_L^n).$$

Using this relation in (3.1e), we get:

$$\forall \sigma = K|L \in \mathcal{E}_{\rm int}, \quad G_{K,\sigma}^{n+1} = (G_{K,\sigma}^{n+1})_{\rm conv} + (G_{K,\sigma}^{n+1})_{\rm diff}, \text{ with}$$

$$(G_{K,\sigma}^{n+1})_{\rm conv} = |\sigma|\ f(p_\sigma^{n+1})\ \tilde{v}_{K,\sigma}^{n+1}, \quad (G_{K,\sigma}^{n+1})_{\rm diff} = \frac{\delta t\ |\sigma|^2}{\rho_{D_\sigma}^n\ |D_\sigma|}\ [f(p_\sigma^{n+1}) + p_K^{n+1}]\ (p_K^{n+1} - p_L^{n+1}),$$

where p_σ^{n+1} stands for the upwind value of p^{n+1} with respect to $u_{K,\sigma}^{n+1}$. On the external faces, still with impermeability conditions, $G_{K,\sigma}^{n+1} = 0$. This nonlinear problem is solved by a quasi-Newton iteration, and the upwinding of p^{n+1} is performed with respect to the normal velocity at the previous Newton

iteration, which does not seem to pose any problem of convergence. The system (C.1) may be seen as a discrete parabolic problem, with a discrete convection-diffusion operator whose diffusion part obeys a Neumann boundary condition (since the flux $(G_{K,\sigma}^{n+1})_{\text{diff}}$ is zero at the external faces). Note that this problem is not conservative (the "diffusion coefficient" is proportional to $f(p_\sigma^{n+1}) + p_K^{n+1}$ on one side of the face and to $f(p_\sigma^{n+1}) + p_L^{n+1}$ on the other side), which is a consequence of the fact that the internal energy balance itself is non-conservative.

When the normal velocity is free at some external face σ, the predicted velocity and the pressure gradient at σ no longer vanish, and we get, denoting by K the cell adjacent to σ:

$$G_{K,\sigma}^{n+1} = \frac{\delta t\ |\sigma|^2}{\rho_{D_\sigma}^n\ |D_\sigma|}\ \left[f(p_K^{n+1}) + p_K^{n+1}\right]\ (p_K^{n+1} - p_{\text{ext}}) + f(p_K^{n+1})\tilde{v}_{K,\sigma}^{n+1},$$

where we have supposed that the flow leaves the domain, so the upwind value for p^{n+1} at σ is p_K^{n+1}, and p_{ext} stands for the external pressure used to approximate the gradient at the face. The discrete diffusion operator for p thus now incorporates an implicit Dirichlet boundary condition on σ.

General case – In the general case, the above-mentioned decoupling of equations in the correction step is not possible, and we use a procedure which is more standard in pressure correction algorithms: as previously, from Equation (3.1c), the end-of-step velocity is written as a function of the end-of-step pressure (and of known quantities), but this expression is now inserted in the mass balance (3.1d), to produce an equation which once again looks like a discrete nonlinear parabolic problem for the pressure, but unfortunately still involves the internal energy, through the computation of the density thanks to the equation of state; then this equation is solved simultaneously with the internal energy balance (3.1e), by a coupled Newton iteration.

This latter algorithm seems rather robust, and has been used for all the tests of this paper; it typically converged in five or less iterations. However, switching to the decoupled version presented for the Euler case sometimes proved useful (in the sense that it allowed significantly greater time steps) in industrial cases, combining stiff shocks with a space grid resolution limited by the computing time; for instance, this was done to compute a jet generated by a leak through a wall separating a low pressure (some Pa) large containment from the outside atmosphere ("loss-of-vacuum" accident scenario in the ITER facility). Note that, whenever the equation of state gives ρe as a function of p only, then the decoupled algorithm may be used even for the general Navier-Stokes equations, at the price of postponing the treatment of the diffusion in the internal energy balance to an additional step of the algorithm.

References

[1] H. Bijl and P. Wesseling. A unified method for computing incompressible and compressible flows in boundary-fitted coordinates. *Journal of Computational Physics*, 141:153–173, 1998.

[2] F. Boyer, F. Dardalhon, C. Lapuerta, and J.-C. Latché. Stability of a Crank-Nicolson pressure correction scheme based on staggered discretizations. *International Journal for Numerical Methods in Fluids*, 74:34–58, 2014.

[3] CALIF3S. A software components library for the computation of reactive turbulent flows. `https://gforge.irsn.fr/gf/project/calif3s`.

[4] V. Casulli and D. Greenspan. Pressure method for the numerical solution of transient, compressible fluid flows. *International Journal for Numerical Methods in Fluids*, 4:1001–1012, 1984.

[5] P. G. Ciarlet. Handbook of numerical analysis volume II : Finite elements methods – Basic error estimates for elliptic problems. In P. Ciarlet and J.L. Lions, editors, *Handbook of Numerical Analysis, Volume II*, pages 17–351. North Holland, 1991.

[6] S. Clain, S. Diot, and R. Loubère. A high-order finite volume method for systems of conservation laws – Multi-dimensional Optimal Order Detection (MOOD). *Journal of Computational Physics*, 230:4028–4050, 2011.

[7] B. Cockburn and C.-W. Shu. The Runge-Kutta Discontinuous Galerkin method for conservation laws V – multidimensional systems. *Journal of Computational Physics*, 141:199–224, 1998.

[8] P. Colella and K. Pao. A projection method for low speed flows. *Journal of Computational Physics*, 149:245–269, 1999.

[9] M. Crouzeix and P.A. Raviart. Conforming and nonconforming finite element methods for solving the stationary Stokes equations. *RAIRO Série Rouge*, 7:33–75, 1973.

[10] F. Dardalhon, J.-C. Latché, and S. Minjeaud. Analysis of a projection method for low-order non-conforming finite elements. *IMA Journal of Numerical Analysis*, 33:295–317, 2013.

[11] P. Drábek and J. Milota. *Methods of Nonlinear Analysis*. Birkhäuser Advanced Texts. Basel Lehrbücher, 2007.

[12] R. Eymard, T. Gallouët, and R. Herbin. Finite volume methods. In P. Ciarlet and J.L. Lions, editors, *Handbook of Numerical Analysis, Volume VII*, pages 713–1020. North Holland, 2000.

[13] L. Gastaldo, R. Herbin, W. Kheriji, C. Lapuerta, and J.-C. Latché. Staggered discretizations, pressure correction schemes and all speed barotropic flows. In *Finite Volumes for Complex Applications VI - Problems & Perspectives - Prague, Czech Republic*, volume 2, pages 39–56. Springer, 2011.

[14] L. Gastaldo, R. Herbin, and J.-C. Latché. A discretization of the phase mass balance in fractional step algorithms for the drift-flux model. *IMA Journal of Numerical Analysis*, 31:116–146, 2011.

[15] J.-L. Guermond and L. Quartapelle. A projection FEM for variable density incompressible flows. *Journal of Computational Physics*, 165:167–188, 2000.

[16] J.L. Guermond, R. Pasquetti, and B. Popov. Entropy viscosity method for nonlinear conservation laws. *Journal of Computational Physics*, 230:4248–4267, 2011.

[17] F.H. Harlow and A.A. Amsden. Numerical calculation of almost incompressible flow. *Journal of Computational Physics*, 3:80–93, 1968.

[18] F.H. Harlow and A.A. Amsden. A numerical fluid dynamics calculation method for all flow speeds. *Journal of Computational Physics*, 8:197–213, 1971.

[19] F.H. Harlow and J.E. Welsh. Numerical calculation of time-dependent viscous incompressible flow of fluid with free surface. *Physics of Fluids*, 8:2182–2189, 1965.

[20] R. Herbin, W. Kheriji, and J.-C. Latché. On some implicit and semi-implicit staggered schemes for the shallow water and euler equations. *Mathematical Modelling and Numerical Analysis*, 48:1807–1857, 2014.

[21] R. Herbin and J.-C. Latché. Kinetic energy control in the MAC discretisation of the compressible Navier-Stokes equations. *International Journal of Finite Volumes*, 7, 2010.

[22] R. Herbin, J.-C. Latché, and T.T. Nguyen. On some consistent explicit staggered schemes for the shallow water and euler equations. *under revision*, 2016.

[23] R. Herbin, J.-C. Latché, and C. Zaza. A cell-centered pressure correction scheme for the compressible Euler equations. *under revision*, 2016.

[24] R.I. Issa. Solution of the implicitly discretised fluid flow equations by operator splitting. *Journal of Computational Physics*, 62:40–65, 1985.

[25] R.I. Issa, A.D. Gosman, and A.P. Watkins. The computation of compressible and incompressible recirculating flows by a non-iterative implicit scheme. *Journal of Computational Physics*, 62:66–82, 1986.

[26] K.C. Karki and S.V. Patankar. Pressure based calculation procedure for viscous flows at all speeds in arbitrary configurations. *AIAA Journal*, 27:1167–1174, 1989.

[27] W. Kheriji. *Méthodes de correction de pression pour les équations de Navier-Stokes compressibles*. Thèse de mathématiques appliquées, Université de Provence, 2011.

[28] W. Kheriji, R. Herbin, and J.-C. Latché. Pressure correction staggered schemes for barotropic monophasic and two-phase flows. *Computers & Fluids*, 88:524–542, 2013.

[29] A. Kurganov and E. Tadmor. Solution of two-dimensional Riemann problems for gas dynamics without Riemann problem solvers. *Numerical Methods for Partial Differential Equations*, 18:584–608, 2002.

[30] N. Kwatra, J. Su, J.T. Grétarsson, and R. Fedkiw. A method for avoiding the acoustic time step restriction in compressible flow. *Journal of Computational Physics*, 228:4146–4161, 2009.

[31] B. Larrouturou. How to preserve the mass fractions positivity when computing compressible multi-component flows. *Journal of Computational Physics*, 95:59–84, 1991.

[32] P. Lax and X.-D. Liu. Solution of two-dimensional riemann problems of gas dynamics by positive schemes. *SIAM Journal on Scientific Computing*, 19:319–340, 1998.

[33] C. Liu and N.J. Walkington. Convergence of numerical approximations of the incompressible Navier-Stokes equations with variable density and viscosity. *SIAM Journal on Numerical Analysis*, 45:1287–1304, 2007.

[34] J.J. McGuirk and G.J. Page. Shock capturing using a pressure-correction method. *AIAA Journal*, 28:1751–1757, 1990.

[35] S. Minjeaud. An unconditionally stable uncoupled scheme for a triphasic Cahn-Hilliard/Navier-Stokes model. *Numerical Methods for Partial Differential Equations*, 29:584–618, 2013.

[36] K. Nerinckx, J. Vierendeels, and E. Dick. Mach-uniformity through the coupled pressure and temperature correction algorithm. *Journal of Computational Physics*, 206:597–623, 2005.

[37] K. Nerinckx, J. Vierendeels, and E. Dick. A Mach-uniform algorithm: coupled versus segregated approach. *Journal of Computational Physics*, 224:314–331, 2007.

[38] L. Piar, F. Babik, R. Herbin, and J.-C. Latché. A formally second order cell centered scheme for convection-diffusion equations on general grids. *International Journal for Numerical Methods in Fluids*, 71:873–890, 2013.

[39] R. Rannacher and S. Turek. Simple nonconforming quadrilateral Stokes element. *Numerical Methods for Partial Differential Equations*, 8:97–111, 1992.

[40] M. Schäfer and S. Turek. *Benchmark Computations of Laminar Flow Around a Cylinder*, volume 52 of *Notes on Numerical Fluid Mechanics*. Vieweg, 1996.

[41] C.W. Schulz-Rinne, J.P. Collins, and H.M. Glaz. Numerical solution of the Riemann problem for two-dimensional gas dynamics. *SIAM Journal on Scientific Computing*, 14:1394–1414, 1993.

[42] D.R. Van der Heul, C. Vuik, and P. Wesseling. Stability analysis of segregated solution methods for compressible flow. *Applied Numerical Mathematics*, 38:257–274, 2001.

[43] D.R. Van der Heul, C. Vuik, and P. Wesseling. A conservative pressure-correction method for flow at all speeds. *Computers & Fluids*, 32:1113–1132, 2003.

[44] J.P. Van Dormaal, G.D. Raithby, and B.H. McDonald. The segregated approach to predicting viscous compressible fluid flows. *Transactions of the ASME*, 109:268–277, 1987.

[45] D. Vidović, A. Segal, and P. Wesseling. A superlinearly convergent Mach-uniform finite volume method for the Euler equations on staggered unstructured grids. *Journal of Computational Physics*, 217:277–294, 2006.

[46] C. Wall, C.D. Pierce, and P. Moin. A semi-implicit method for resolution of acoustic waves in low Mach number flows. *Journal of Computational Physics*, 181:545–563, 2002.

[47] I. Wenneker, A. Segal, and P. Wesseling. A Mach-uniform unstructured staggered grid method. *International Journal for Numerical Methods in Fluids*, 40:1209–1235, 2002.

[48] P. Woodward and P. Colella. The numerical simulation of two-dimensional fluid flow with strong shocks. *Journal of Computational Physics*, 54:115–173, 1984.

[49] Z. Xu, Y. Liu, H. Du, G. Lin, and C.-W. Shu. Point-wise hierarchical reconstruction for discontinuous Galerkin and finite volume methods for solving conservation laws. *Journal of Computational Physics*, 230:6843–6865, 2011.

[50] S.Y. Yoon and T. Yabe. The unified simulation for incompressible and compressible flow by the predictor-corrector scheme based on the CIP method. *Computer Physics Communications*, 119:149–158, 1999.